

AD-A151 928



Reproduced From
Best Available Copy

AN EMPIRICAL SELF-PROTECTION

CHAFF MODEL

THESIS

Robert J. Rohrs
First Lieutenant, USAF

AFIT/GP/ENG/340-54

This document has been approved
for release and sale in
discreet quantities.

DTIC FILE COPY

DTIC
SELECTED
APR 02 1985
S D E

DEPARTMENT OF THE AIR FORCE
AIR UNIVERSITY

AIR FORCE INSTITUTE OF TECHNOLOGY

Wright-Patterson Air Force Base, Ohio

20000807031

85 08 13 052

DISCLAIMER NOTICE

**THIS DOCUMENT IS BEST QUALITY
PRACTICABLE. THE COPY FURNISHED
TO DTIC CONTAINED A SIGNIFICANT
NUMBER OF PAGES WHICH DO NOT
REPRODUCE LEGIBLY.**

AFIT/GE/ENG/84D-54

Copy available to DTIC does not
permit fully legible reproduction

AN EMPIRICAL SELF-PROTECTION

CHAFF MODEL

THESIS

Robert J. Rohrs
First Lieutenant, USAF

AFIT/GE/ENG/84D-54

APR 02 1985

E

Approved for public release; distribution unlimited

AN EMPIRICAL SELF-PROTECTION

CHAFF MODEL

THESIS

Presented to the Faculty of the School of Engineering

of the Air Force Institute of Technology

Air University

In Partial Fulfillment of the

Requirements for the Degree of

Master of Science in Electrical Engineering

Robert J. Rohrs

First Lieutenant, USAF

December 1984



Accession For		
AFIT/GE/ENG/84D-54		<input checked="" type="checkbox"/>
AFIT/GE/ENG/84D-54		<input type="checkbox"/>
AFIT/GE/ENG/84D-54		<input type="checkbox"/>
By		
Distribution /		
Availability Codes		
and/or		
Special		
A-1		23 E12

Approved for public release; distribution unlimited

Preface

The purpose of this study was to develop a computer model to calculate the probability of attaining breaklock in an aircraft-chaff-tracking radar encounter. Although some of the assumptions made may seem to oversimplify the model, these were necessary to create the simple, quick running simulation that was desired. p vii

In creating the simulation and writing this thesis I owe a special thanks to those who have come to my aid. I am extremely thankful that I was able to tap such a beneficial resource as my advisor, Dr. V.P. Pyati. I also wish to express my thanks to Capt T.W. Johnson, recently departed from AFIT, and Mr. Robert Puskar, formerly of AFAL/WRP-3, for their help and guidance in getting this project underway.

My deepest gratitude goes to my wife, Nancy, and son, Peter, for their encouragement and understanding while enduring the hardships that an AFIT assignment can place on a family.

Table of Contents

	Page
Preface	ii
List of Figures	iv
List of Tables	vi
Abstract	vii
I. Introduction	1
II. Background Theory	4
Chaff	4
Mature Chaff Clouds	5
Immature Chaff Clouds	9
Aircraft	11
Scan with Compensation Radar	14
III. Centroid Tracking Model	30
Simple Tracking Model	30
FTI Radar Model	36
IV. Model Simulation	39
Input Variables	39
Locations	40
MTI Response	45
V. Conclusions and Recommendations	54
Bibliography	59
Vita	61

List of Figures

Figure	Page
1. Spectrum Width due to Wind Shear	8
2. Measured Aircraft RCS vs. Aspect Angle	12
3. Smoothed Data from Figure 2	13
4. Scan with Compensation Radar	15
5. Error Voltage Generation (Target on Boresight)	16
6. Error Voltage Generation (Target off Boresight)	18
7. Error Voltage Generation (Target off Boresight, with Jamming)	19
8. Error Voltage Generation (Two Targets Equidistant from Boresight)	20
9. Single Delay-Line Canceler	21
10. Frequency Response of Single Delay-Line Canceler	22
11. Single vs. Double Cancellation	22
12. Composite Frequency Response of Single Delay-Line Canceler	23
13. IF Automatic Gain Control	24
14. Split-Range-Gate Tracking	25
15. Range Gate Model	26
16. Type II Range Servo	27
17. Angle Error Voltage Generation	28
18. Radar Resolution Cell	31
19. SWC Power Pattern	34
20. SWC Radar	37
21. Aircraft Radial and Tangential Velocity Components	43
22. Simulation MTI Filter Response	46

List of Figures (Cont.)

Figure	Page
23. Simulation Flow Chart	51-53
24. Simulation #1 Results	55
25. Simulation #2 Results	56

List of Tables

Table		Page
1.	Wire Lengths Required to Produce Resonant Half-Wave Dipoles for a Wire of Length L and Diameter d . . .	5
2.	Variance Components due to Beam Broadening, Turbulence, and Fall Rate	9
3.	Simulation Input Parameters Describing the Aircraft, Chaff, and Radar	41
4.	Simulation Inputs	55

Abstract

This thesis produced a simulation capable of charting the effectiveness of chaff used in the self-protective mode. Simulation results can be used to determine which type/design of chaff/chaff canister will produce a greater probability of breaklock for a given scenario.

The radar included in this simulation is a Scan with Compensation tracking radar. Variable parameters include pulse width, beamwidth, pulse repetition frequency, and operation frequency. An "ideal" MTI filter is incorporated into the model to negate the effects of MTI blind speeds.

Results of several simulation runs illustrate the effects of varying chaff radar cross section and aircraft velocity on the probability of attaining breaklock. Although aircraft maneuvers are not included in the simulation, conclusions as to how the probability of breaklock is affected can be made by varying the velocity vector.

*Additional
Remarks: Survivability, combat aircraft.*

AIR FORCE ELECTRONIC SELF-PROTECTION

CHAFF MODEL

1. Introduction

Chaff has been used as a passive radar countermeasure since World War II. Even in the sophisticated Electronic Warfare (EW) environment that exists today, chaff by itself or in conjunction with other countermeasures can increase the survivability of aircraft in combat.

However, chaff's effectiveness can be diminished by sophisticated radar techniques. Furthermore, because of space and weight limitations, only a finite amount of chaff can be carried on a given aircraft. The purpose of this thesis is to develop a computer program to calculate the probability of breaklock in an aircraft-chaff-tracking radar encounter. In particular, the computer program will evaluate the effectiveness of chaff for a given set of input parameters such as radar characteristics, type of aircraft, and scenario. This will, hopefully, enable a pilot to choose the best possible chaff dispensing tactics.

Background

The Air Force Electronic Warfare Center (AFEWC) is frequently required to perform analysis to determine the relative effectiveness of Electronic Combat (EC) systems. Present self-protective chaff analysis is limited to the Simulated Chaff/ Aircraft/ Radar Encounter (SCARE) (Bang, 1979:47-68) program. This program, in its present form, is not suitable to the needs of AFENC. The AFENC has expressed a desire for a computer model that will meet its needs.

Problem

To produce a computer model that will overcome the deficiencies of the SCARE program and generate more efficient models of the radar, chaff, and/or aircraft. In addition, the outputs of these models need to be processed to produce the desired probability of attaining break-lock.

Scope

This study is limited to a single aircraft/chaff/Scan-with-Compensation (SWC) tracking radar encounter. The SWC radar has moving target indication (MTI) capability and automatic gain control (AGC) networks. Pulse repetition frequency (PRF) agility/staggering will be limited to the ability to eliminate signal degradation at multiples of the PRF. No human operator functions will be contained in the loop.

The aircraft will be incapable of evasive maneuvering. Chaff will be the only electronic combat option available to the aircraft. Active jamming will not be considered, although useful conclusions may be drawn as to how jamming could further enhance chaff effectiveness.

Approach

The SCARE computer simulation was examined for possible modification to produce the desired output. The size and complexity of the simulation rendered this approach unfeasible.

A simple chaff/aircraft/radar, power-centroid tracking scenario was then expanded to include immature chaff cloud properties and typical SWC radar characteristics.

In an effort to reduce both the number of input variables and the

complexity of the situation, servo system tracking loops were assumed ideal.

Sequence of Presentation

Chapter II develops the theory of chaff, SWC radar, and aircraft radar cross section and Doppler frequency characteristics. It is assumed that the reader is familiar with these topics and only the features of each topic which have an impact on the simulation will be discussed. Chapter III presents a power-centroid tracking model and discusses the effect of certain radar characteristics on the model. In Chapter IV, the properties outlined in Chapter II are integrated into the model from Chapter III. Conclusions and recommendations are contained in Chapter V.

11. Background Theory

Chaff

Chaff can be employed in either a screening or a self-protective mode. In the screening role, chaff dispensing airplanes fly ahead of the attacking aircraft. Chaff is dropped continuously to form a "corridor" to hide the attacking formation. When the attacking aircraft enter the corridor, they are screened from the radar due to the large radar cross section (RCS) presented by the chaff cloud.

Self-protective chaff is employed to transfer, or break, radar lock from a target. This method is used against a tracking radar, as it is only effective when the aircraft and chaff are within the same radar resolution cell. Chaff, in this role, has not reached the "steady-state" (mature) conditions of the chaff in the screening role. The characteristics of "immature" chaff clouds are important factors in the attempt to achieve break-lock. While this report is mainly concerned with immature chaff clouds, a review of physical characteristics and mature chaff clouds is helpful.

Physical Characteristics

Single chaff dipoles are constructed of metal (usually aluminum), or metal-coated glass or nylon. Aluminum chaff comes in flat strips while glass chaff is round, resembling a strand of hair. The length of a dipole is approximately one-half wavelength of the radar operating frequency. Actual length at resonance is a function of the length-to-diameter ratio. Table 1 lists resonant lengths of several dipole classes.

Table 1. Wire lengths required to produce a resonant half-wave dipole for a wire of diameter d and length L (Stutzman and Thiele, 1981:202)

L/d	percent shortening required	resonant length L	dipole thickness class
5000	2	0.49λ	very thin
50	5	0.475λ	thin
10	9	0.455λ	thick

Nature Chaff Clouds

Nature chaff clouds are those clouds that have reached a "steady-state". That is, the dipoles within the cloud are well dispersed and their motion is dependent on local wind currents. Maturity is reached after the cloud has been allowed to "settle" for several minutes.

Radar Cross Section. The radar cross section of an object is 4 π times the power reflected toward the source per unit solid angle divided by the incident power density on the target (Skolnik, 1980:33). The RCS of a single chaff dipole, assuming resonant length, is approximately (Barrick, 1970:300):

$$\sigma = 0.86\lambda^2 \cos^2 \gamma_i \cos^2 \gamma_s \frac{\cos(\pi/2(\sin \psi_i))^2}{\cos^2 \psi_i} \frac{\cos(\pi/2(\sin \psi_s))^2}{\cos^2 \psi_s} \quad (1)$$

where λ is the wavelength of the incident signal and γ_i , ψ_i , γ_s , and ψ_s are the angles of polarization and orientation of the dipole to the transmitted wave for the incident and scattered fields, respectively.

From equation (1), it is obvious that the maximum RCS occurs when all

angles are zero; giving a value of:

$$\sigma = 0.86 \lambda^2 \quad (2)$$

At the other extreme, when the dipole is oriented parallel to the radar wave's direction of propagation, the RCS is zero. The average RCS, over all possible dipole orientations is (ibid:300):

$$\sigma_{avg} = 0.155 \lambda^2 \quad (3)$$

Assuming all dipoles are of length $\lambda/2$, the RCS of a chaff cloud is dependent on the orientation of the dipoles within. For well dispersed clouds, the amplitude and phase signals from each dipole are independent (Bang, 1979:5). It has been shown that for a cloud containing as few as five dipoles, the central limit theorem can be invoked to determine the statistics of chaff cloud scattering (Pyati, 1975). The probability density function of the RCS (σ) can be shown to be:

$$f(\sigma) = (1/\sigma_0) \exp(-\sigma/\sigma_0) \quad (4)$$

where σ_0 is the expected or average RCS value.

During the first few moments after dispersion, dipole interaction affects the RCS of the chaff cloud. The RCS of the chaff cloud is now modeled as (Golden, 1983:172):

$$\sigma = A_c [1 - \exp(-n \sigma_{avg})] \quad (5)$$

where A_c is the two-dimensional vertical size of the cloud area illuminated by the radar and n is the number of dipoles per unit area. If $n \sigma_{avg}$ is large, the RCS equals A_c , while after the dipoles "settle"

as σ_{avg} becomes small, reducing equation (5) to (ibid:172):

$$\sigma = N \sigma_{\text{avg}} = N(0.155 \lambda^2) \quad (6)$$

where N is the number of dipoles within the cloud. Therefore, equation (6) is the RCS of a mature chaff cloud.

Doppler. The fluctuations of the RCS of a mature chaff cloud are due to the relative motion of the dipoles within the cloud. This motion is caused by wind shear, turbulence, fall rate, and beam broadening (Nathanson, 1969:224). The doppler spectrum is generally Gaussian in shape, with the mean a function of the radial velocity of the cloud as it drifts along and a variance due to internal motion of the dipoles.

The mean doppler frequency is given by the familiar formula:

$$f_d = (2/\lambda) v_{r\text{wind}} \quad (7)$$

and the variance is (ibid:227):

$$\sigma_f^2 = \frac{4f_o^2}{c^2} \sigma_v^2 \quad (8)$$

where f_o is the radar operating frequency and σ_v is given by:

$$\sigma_v^2 = \sigma_{\text{shear}}^2 + \sigma_{\text{beam}}^2 + \sigma_{\text{turb}}^2 + \sigma_{\text{fall}}^2 \quad (9)$$

σ_{shear} is a function of the radar antenna elevation beamwidth and range, and is plotted in Figure 1. The variances due to the other causes are listed in Table 2. Nathanson estimates σ_v^2 to lie within a range of 0.36-1.7 m^2/sec^2 (ibid:255). At an f_o of 7 GHz, the frequency variance

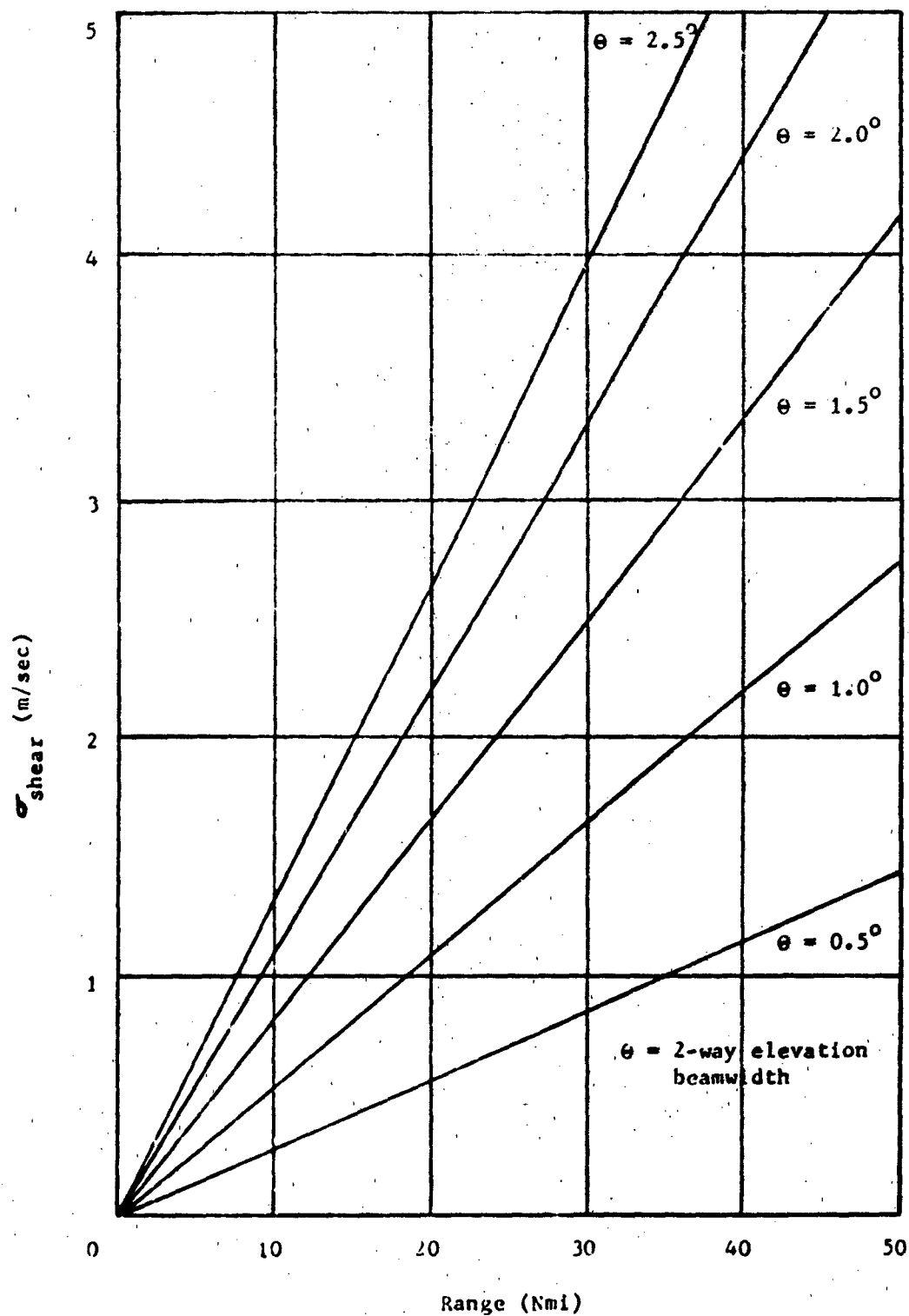


Fig.1. Spectrum Width due to Wind Shear (average over 360° of azimuth)
(Nathanson, 1969:208)

Table 2. Variance components due to beam broadening, turbulence, and fall rate.
(ibid:Ch 6)

σ_{beam}^2	less than $0.25 \text{ m}^2/\text{sec}^2$
σ_{turb}^2	$1.0 \text{ m}^2/\text{sec}^2$ (below 12,000 ft) $0.49 \text{ m}^2/\text{sec}^2$ (above 12,000 ft)
σ_{fall}^2	$0.2025 (\sin \psi)^2 \text{ m}^2/\text{sec}^2$ $\psi = \text{elevation angle}$

of the chaff doppler spectrum would range from 784 to 3702 Hz.

The chaff power spectrum is now given as (Barlow, 1949:351):

$$G(f) = G_0 \exp \left[-(f-f_d)^2 / 2 \sigma_f^2 \right] \quad (10)$$

where G_0 is a constant dependent on the average received power.

Immature Chaff Clouds

The characteristics of immature chaff clouds are not well understood because it is difficult to obtain reliable measurements. Cloud measurements are corrupted due to wave scattering from the aircraft and by aircraft turbulence. The RCS and doppler characteristics are different from those of a mature cloud due to the dense mass of dipoles and the initial velocity imparted by the dispensing aircraft.

Radar Cross Section. The RCS of an immature chaff cloud is time dependent due to the growth in the cloud area as the chaff spreads. Coupled with the fact that individual dipoles are partially shielded

by other dipoles, one can show that the RCS of an immature cloud has, approximately, an exponential rise. One has:

$$\sigma(t) = \sigma_{\max} [1 - \exp(-t/\tau_\sigma)] \quad (11)$$

where τ_σ is the bloom rate. At $t = 3\tau_\sigma$, $\sigma(t) = 0.95 \sigma_{\max}$. Therefore, a fast bloom rate allows $\sigma(t)$ to approach σ_{\max} quickly.

Doppler. As stated previously, accurate chaff statistics are difficult to measure for immature clouds. Since the variance of the doppler spectrum is dependent on turbulence, the total variance cannot be calculated without accurate data. For purposes of this report, the effect of aircraft turbulence on σ will be assumed negligible.

The mean of the doppler spectrum for an immature cloud is significantly different from the statistics of a mature cloud. The mean is not only dependent on the wind's radial velocity, but has an exponential decay as a function of time. The time-varying velocity component can be expressed as:

$$v(t) = v_0 \exp(-t/\tau_v) \quad (12)$$

where τ_v is the chaff deceleration constant. Chaff elements having a small aerodynamic drag (increased τ_v) will maintain a significant mean in the doppler spectrum for a longer period of time.

Applying equation (10) to an immature chaff cloud yields a power spectrum of ($v_{\text{wind}}=0$):

$$G(f) = \sigma_0 \exp \left[-((f - f_d(t))^2 / 2 \sigma_f^2) \right] \quad (13)$$

where $f_d(t)$ is given by:

$$f_d(t) = (2/\lambda) v_r(t) \quad (14)$$

Aircraft

Radar Cross Section. The RCS of an aircraft is highly dependent upon the radar viewing angle (See Figure 2). As shown, a slight change in aspect (viewing) angle can contribute to a large change in RCS. The "smoothed" data of Figure 3 is a more usable representation of the actual RCS. Since only the peak information is used, it also represents "worst case" data. In all probability, the actual RCS will be smaller than the RCS used from the smoothed data.

The fine grain structure of Figure 2 is due to constructive and destructive interference of multiple scatterers on a complex body such as an aircraft. Changes in aspect angle occur as an aircraft moves along its path, creating an RCS which appears to be time-varying. For practical purposes, and for this report, the RCS of the aircraft is the mean of the distribution of the RCS over all viewing angles.

Doppler. The effect of multiple scatterers in motion causes a change in doppler frequency. Therefore, as the viewing angle of an aircraft changes, the multiple scatterers which make up an aircraft cause a shift in doppler frequency. This effect can be negated, however, by assuming an aircraft is a point target. The doppler frequency of the aircraft is now due only to the radial velocity and can be represented as stated in equation (14).

RCS OF A B-26 AT 3GHz

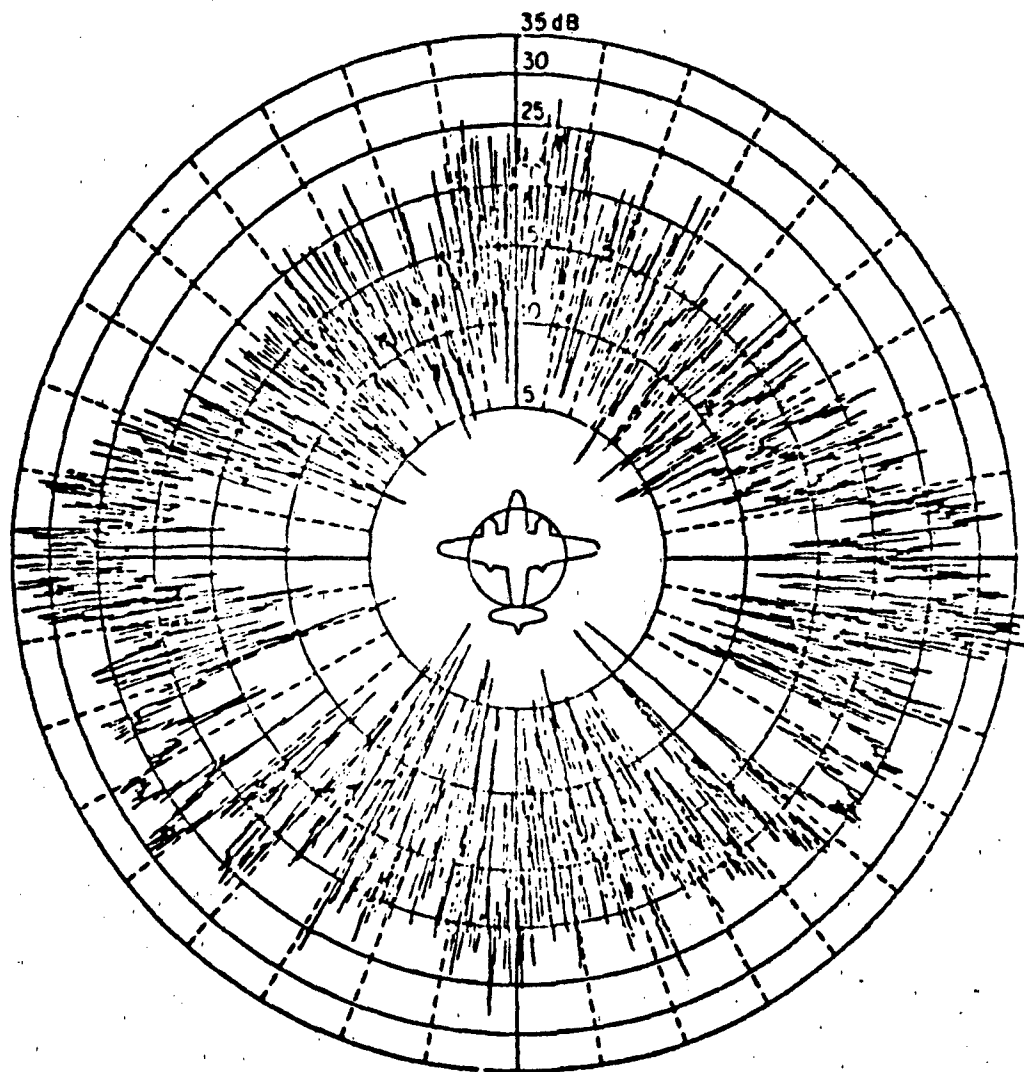


Fig 2. Measured RCS vs. Aspect Angle (Johnson, 1983)

"SMOOTHED" RCS DATA

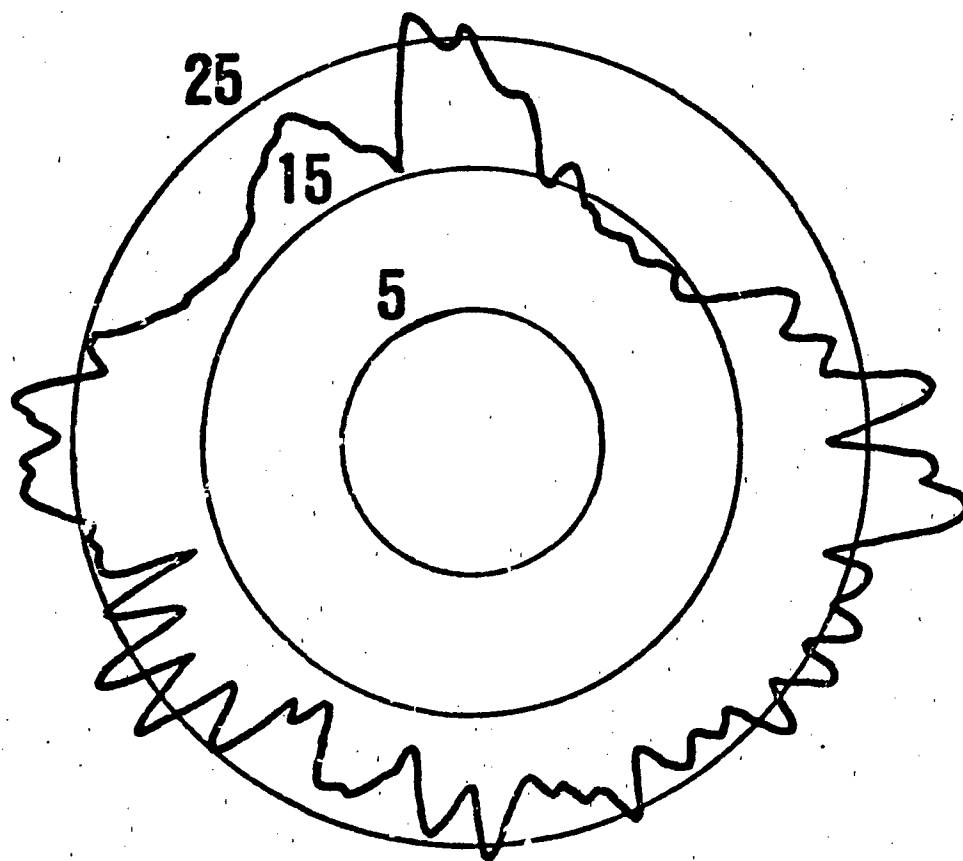


Fig 3. Smoothed Data from Figure 2 (Johnson, 1983)

Scan with Compensation Radar

Scan with Compensation (SWC) radar is a conical scan tracking radar employing dual receive beams (Van Brunt, 1982:143). Two simultaneous nutating beams, one transmit and receive, one receive only, are placed so that the return signals are mirror images of each other. The received information from each beam is processed separately, then subtracted at video level to produce an error signal. This error signal is then used to reposition the antenna.

Processing can take place using either two separate receivers or by time-multiplexing the two signals through one receiver. A simplified block diagram of an SWC radar employing separate receivers is shown in Figure 4. SWC radar was originally developed as an ECCM technique against inverse gain jamming.

Error Signal. The error signal output of the subtractor is used to drive the antenna positioning servo-systems. Analysis of the error output for three separate tracking scenarios will establish the theory of operation for an SWC radar.

The first scenario will put a target on the track axis, with no jamming present. In this case, it can be seen from Figure 5 that the error voltage will be zero. As would be expected, the antenna-drive servos receive no signal to reposition the antenna.

Tracking radar theory calls for repositioning of the antenna if the target is off the track-axis. With a target positioned off bore-sight and no jamming present, an error signal is then expected. Analysis of receiver outputs for a target in this position shows that an error voltage is indeed generated to reposition the antenna (See Fig-

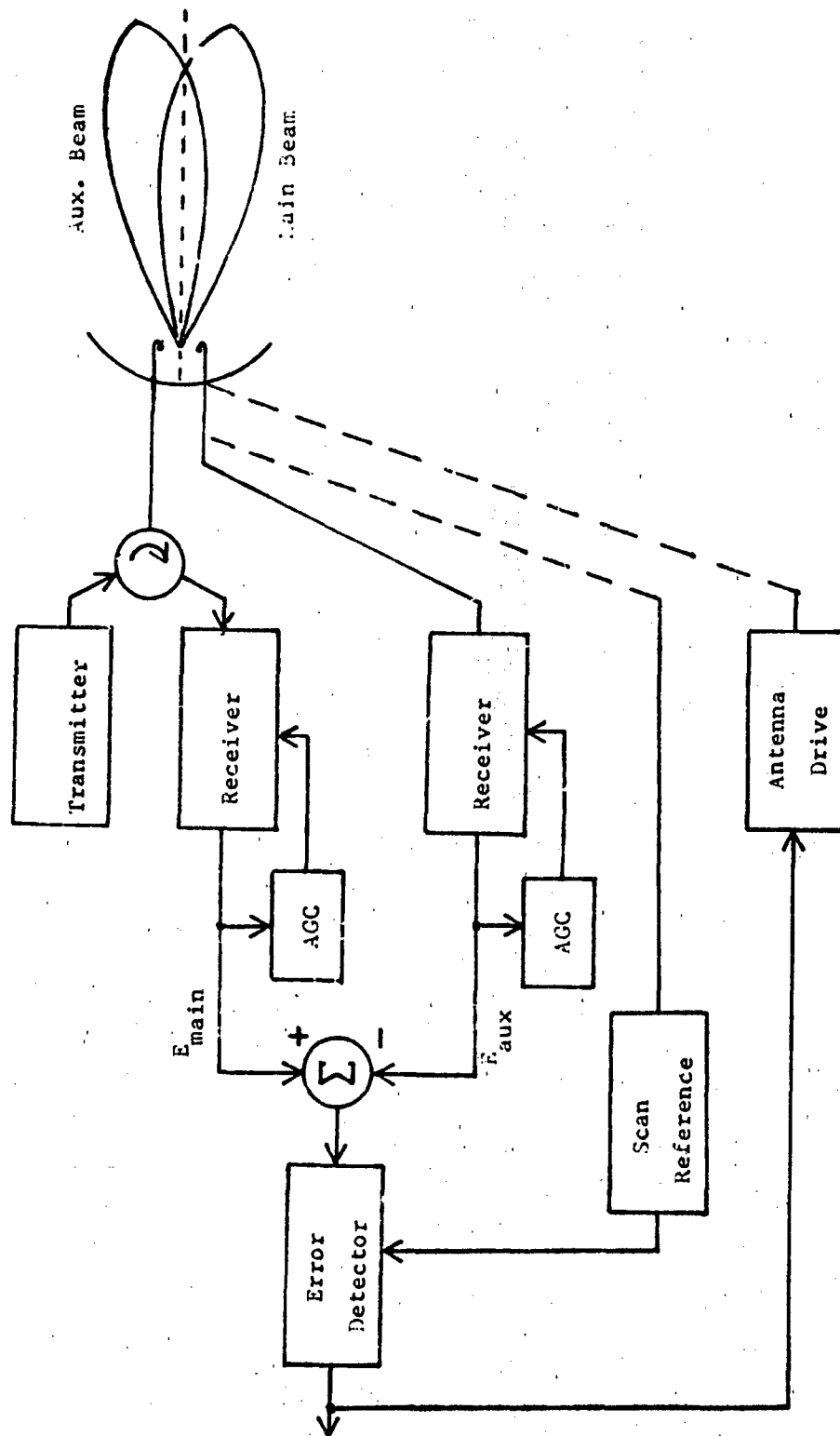


Fig 4. Scan with Compensation Radar (Golden, 1983:Fig. 2-41)

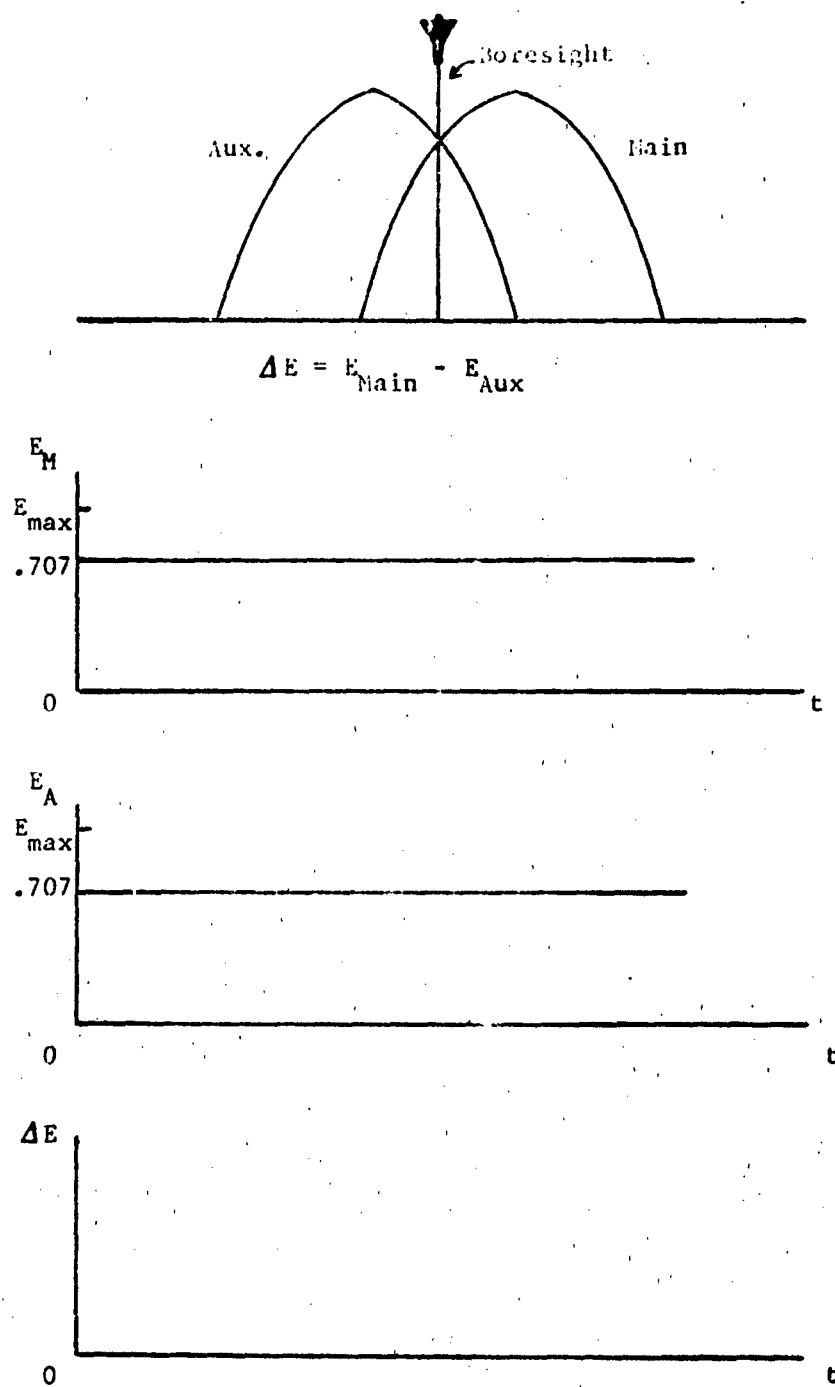


Fig 5. Error Voltage Generation (Target on Boresight)

ure 6).

The last scenario places a target off boresight with a noise jammer of constant amplitude. The receiver outputs are each increased in amplitude by the magnitude of the jamming signal. However, the error voltage remains the same as in the no jamming case, due to the fact that the subtractor cancels inputs common to both channels (See Figure 7). This cancellation effect is what allows the SVC radar to counter the effect of inverse gain jamming on a conical scan radar.

Moving Target Indication. Moving target indication (MTI) is an ECCM technique usually employed in SVC radar. Figure 8 shows the outputs for an aircraft-chaff encounter with an SVC radar without MTI capabilities. An aircraft and a chaff cloud of equal RCS are positioned off boresight at an equal but opposite distance. The outputs of each receiver and the resulting error signal show that without MTI, the radar will continue to track a point between the two targets. In order to successfully track an aircraft in this scenario, the radar must possess the ability to distinguish between an actual target and clutter.

Delay-Line Canceler. A simple MTI filter is the delay-line canceler. The received signal is compared to the signal received from the last received pulse. Since a delay-line canceler is a time-domain filter, this single network operates over all frequency ranges, thereby holding a large advantage over frequency-domain MTI methods (Skolnik, 1980:107).

A single delay-line canceler is shown in Figure 9. The received

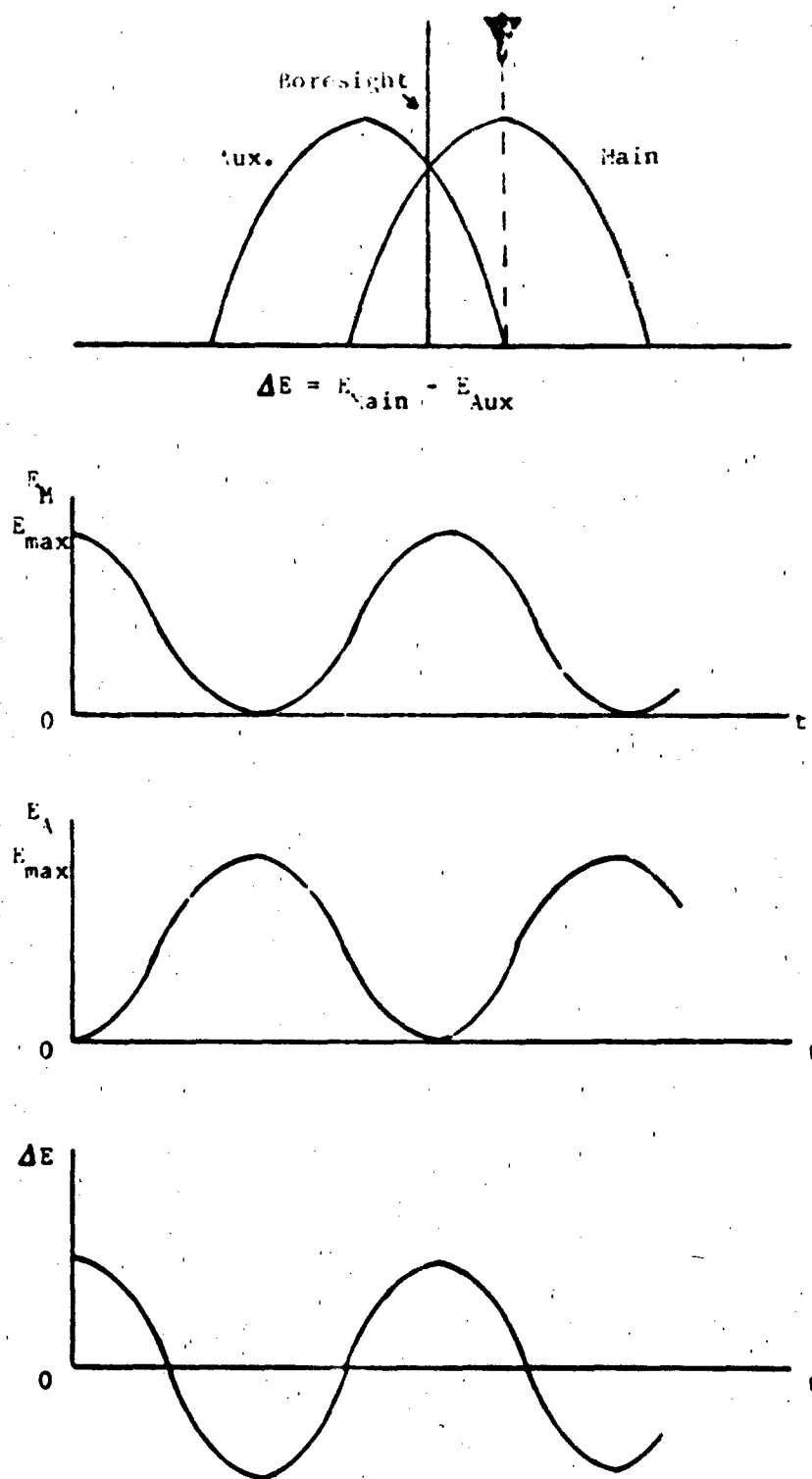


Fig. 6. Error Voltage Generation (Target off Boresight)

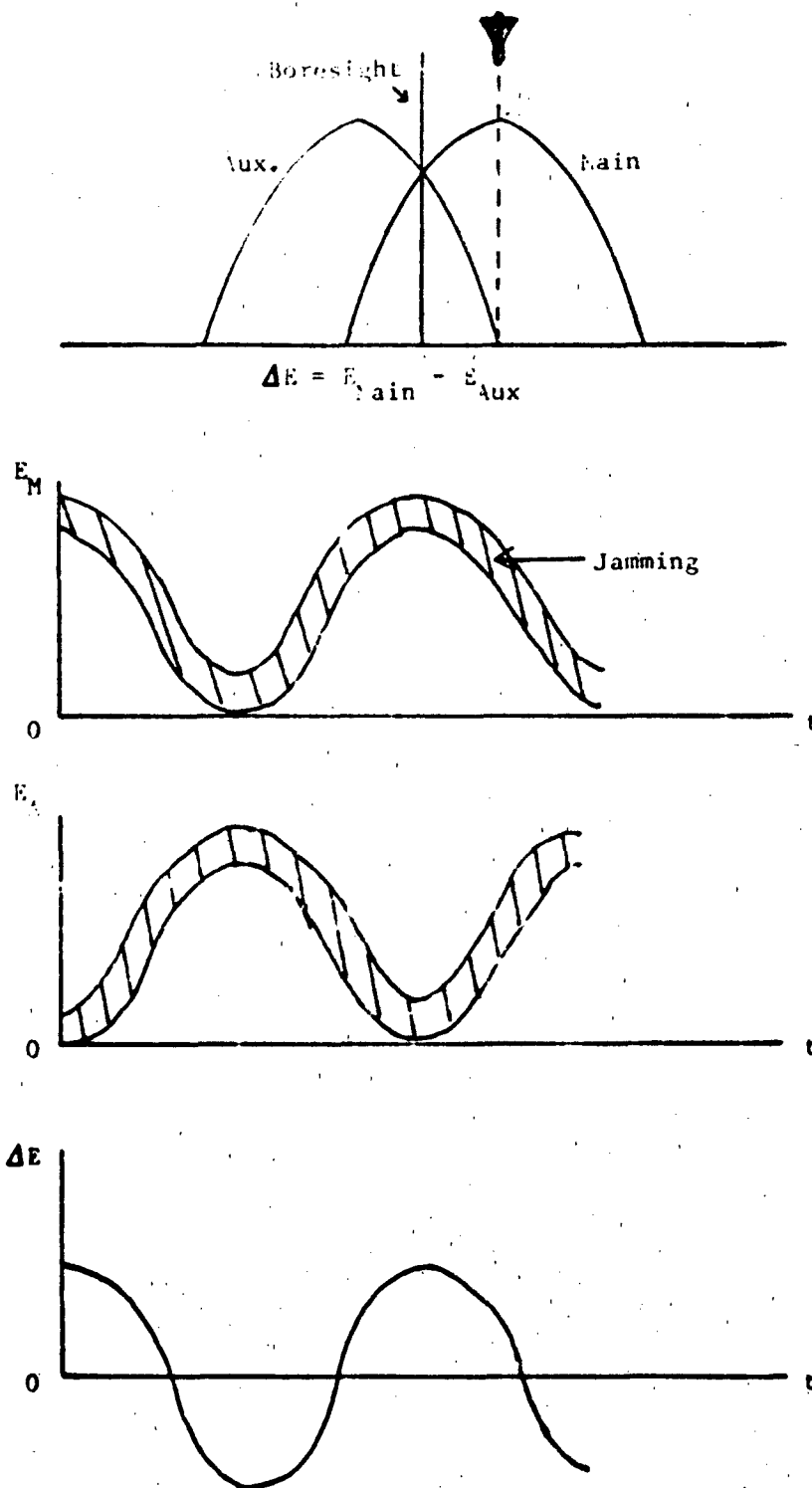


Fig 7. Error Voltage Generation (Target off Boresight with Jamming)

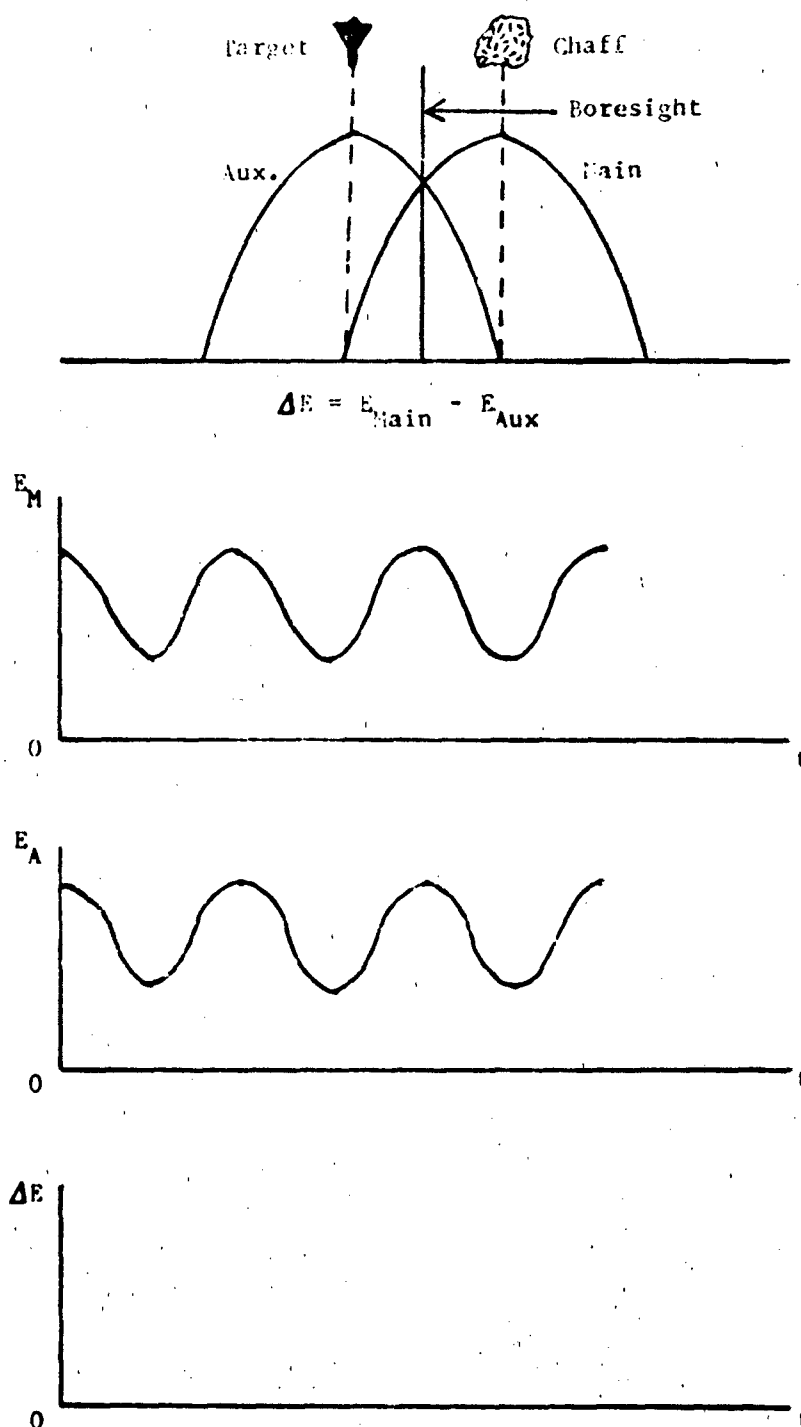


Fig 8. Error Voltage Generation (Two Targets Equidistant from Boresight)

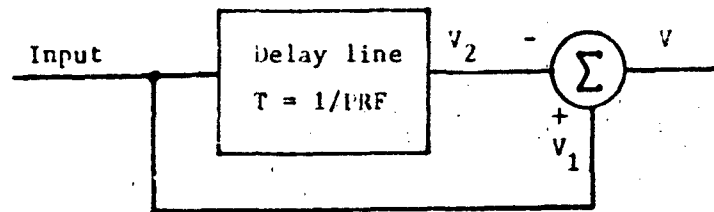


Fig 9. Single Delay-Line Canceler

signal is:

$$V_1 = k \sin(2\pi f_d t - \phi_0) \quad (15)$$

where ϕ_0 is the phase shift and k is the amplitude. The signal from the previous return pulse, time $t-T$, where T is the pulse repetition interval, is:

$$V_2 = k \sin(2\pi f_d (t-T) - \phi_0) \quad (16)$$

The output of the summing junction is given by:

$$V = V_1 - V_2 = 2k \sin(\pi f_d T) \cos[2\pi f_d (t-T/2) - \phi_0] \quad (17)$$

The output is a cosine wave of amplitude $2k \sin(\pi f_d T)$. The magnitude of the frequency response of the single delay-line canceler versus the normal radar video (k) is shown in Figure 10. Normal clutter has a doppler frequency in the vicinity of zero and is attenuated by the filter. A moving target ($f_d \gg 0$) is amplified by the canceler, except in the vicinity of frequencies that are multiples of the PRF.

The clutter rejection notches of a single delay-line canceler can be broadened by cascading several cancelers. A double delay-line can-

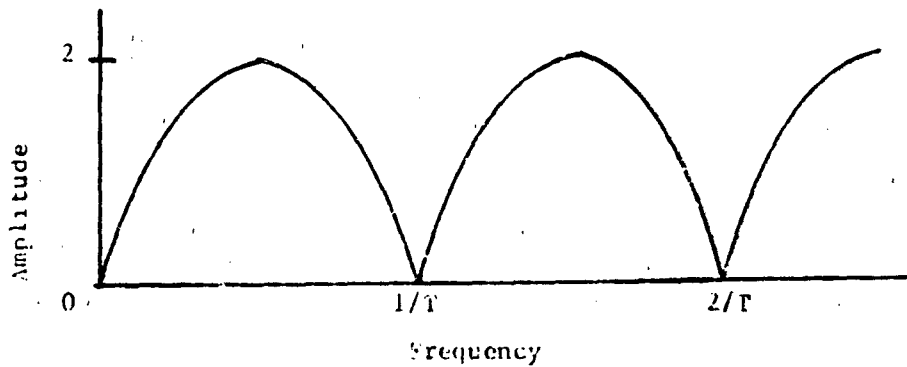


Fig 10. Frequency Response of Single Delay-Line Canceler ($T=1/\text{PRF}$)

celer (two single cancelers in cascade) has a frequency response of (ibid:109):

$$H(f) = 4 \sin^2(\pi f_d T) \quad (18)$$

Figure 11 compares the response of the double delay-line canceler to that of a single canceler.

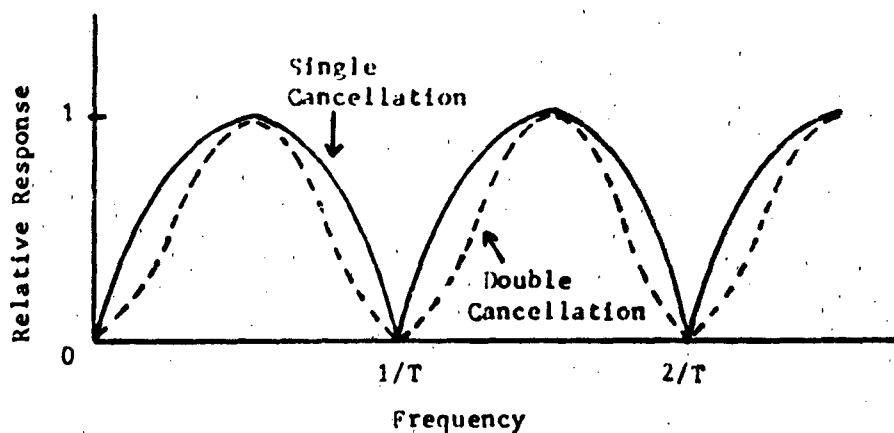


Fig 11. Single versus Double Cancellation

Both cancelers of Figure 11 have unwanted signal attenuation at doppler frequencies that are multiples of the PRF. The velocities that yield signals in these notches are called blind speeds. Since the blind speeds are functions of the PRF, they can be virtually eliminated by switching the PRF from pulse to pulse (staggering). Figure 12 shows the response of a two PRF staggered system. As the number of staggered PRF's increases, the frequency response approaches unity for large bands of frequency.

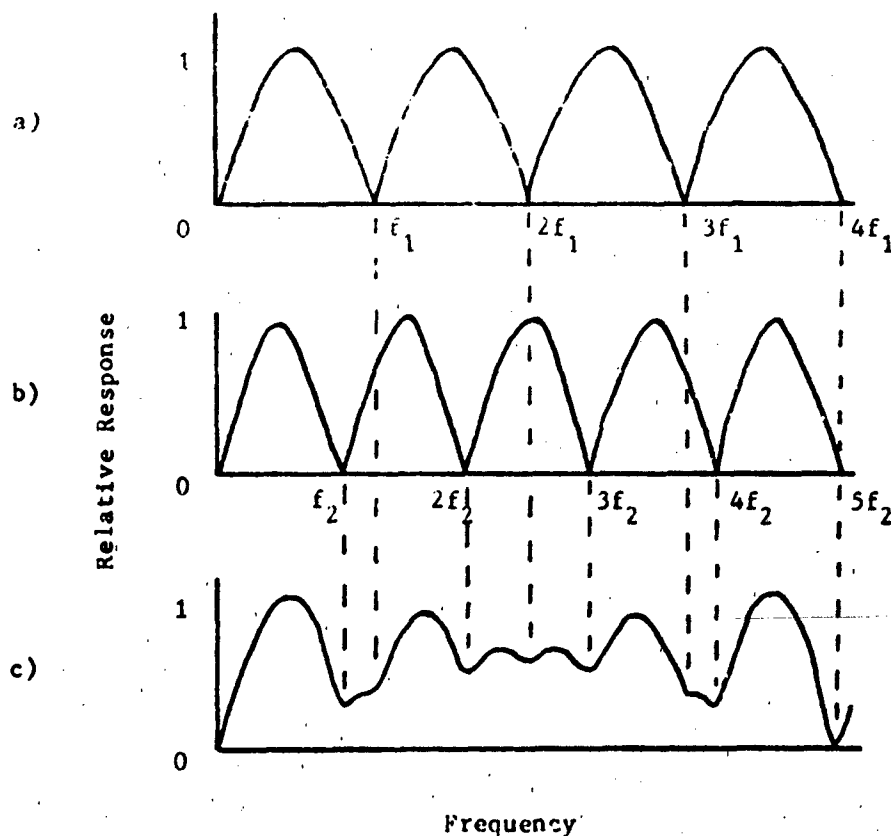


Fig 12. a) Frequency Response of Single Delay-Line Canceler for PRF = f_1 ; b) same for PRF = f_2 ; c) Composite Response with $f_1/f_2 = 4/5$ (Skolnik, 1980:Fig. 4.16)

Automatic Gain Control. Automatic gain control (AGC) is used to maintain the IF amplifier output signal at a constant level over a wide range of values of the received signal (Golden, 1983:278). Noiselike amplitude fluctuations of the error signal are thereby removed, allowing the true error signal to be processed.

AGC is accomplished by controlling the amplifier gain through an AGC control voltage (See Figure 13). A weak input signal produces a small V_{reg} , allowing K to increase. On the other hand, a large input signal produces a large V_{reg} , thereby decreasing K . Operating in this way, an AGC circuit increases the dynamic operating range of a radar receiver.

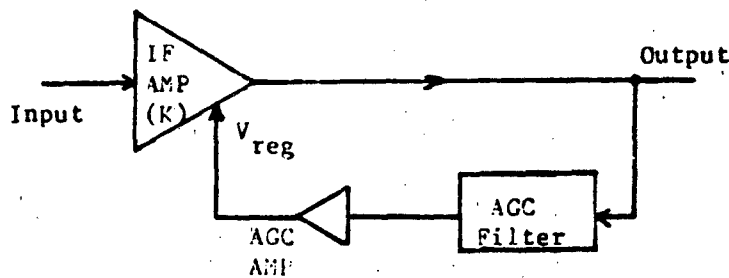


Fig 13. IF Automatic Gain Control

Practical hardware limitations restrict the maximum gain variation to the order of 40db, but the use of multiple IF amplifiers allow the dynamic range to be increased to the order of 90db to allow for fluctuations in the parameters of the radar range equation (Skolnik, 1980: 158).

Although AGC systems are often employed elsewhere in radar receiv-

ers, the basic operation remains the same. Different AGC techniques usually differ in response times. Conventional IF AGC has a response time larger than one conical-scan period, while a fast AGC system responds faster than the conical-scan period, but slower than the pulse repetition period (Van Brunt, 1982:461).

Range Tracking. Range tracking in an SWC radar is accomplished automatically, using split-gate tracking (Vakin and Shustov, 1969:236). Two square pulses, called the early gate and the late gate, are generated by the radar (See Figure 14). T_0 is supplied from the previous

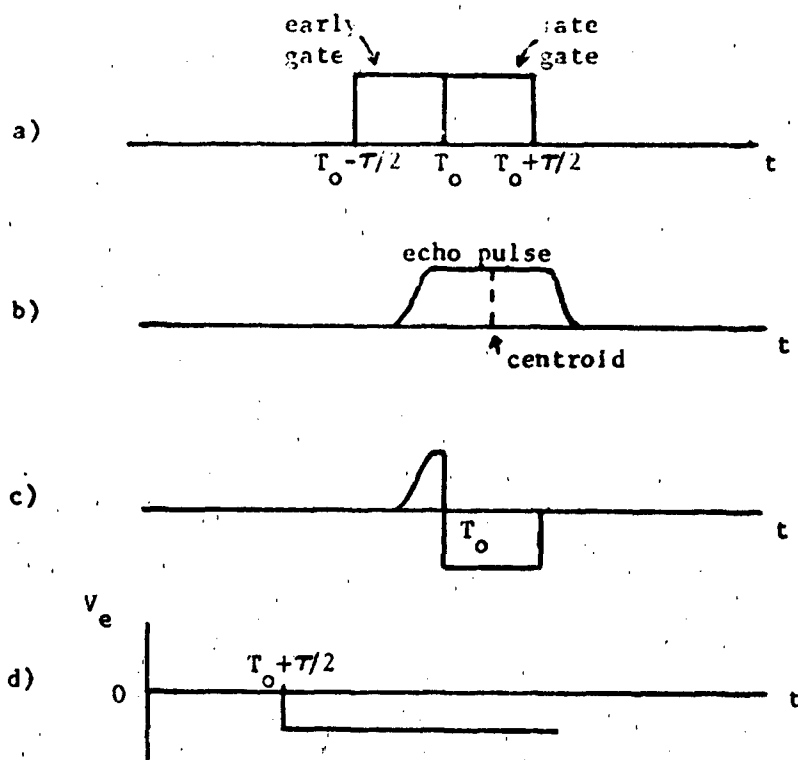


Fig 14. Split-Range-Gate Tracking. a) Early-late range gates; b) echo pulse; c) early gate, late gate signals; d) difference signal (adapted from Skolnik, 1980:Fig. 5.17)

return pulse and τ is the transmitted pulse width. The return pulse from the target is then compared to the gates. If more of the returned energy lies within one gate than another, an error signal is generated and the range (also T_0) is repositioned. If the energies within each gate are equal, the range (and T_0) remains the same.

The error signal can be generated by using two integrators and a subtractor (See Figure 15). The return pulse is integrated from $T_0 - \tau/2$ to T_0 , and from T_0 to $T_0 + \tau/2$. The difference of these two integrands is the error signal. The magnitude of the difference signal measures the distance from the previous range to the new range, while the sign of the error determines the direction of the range change.

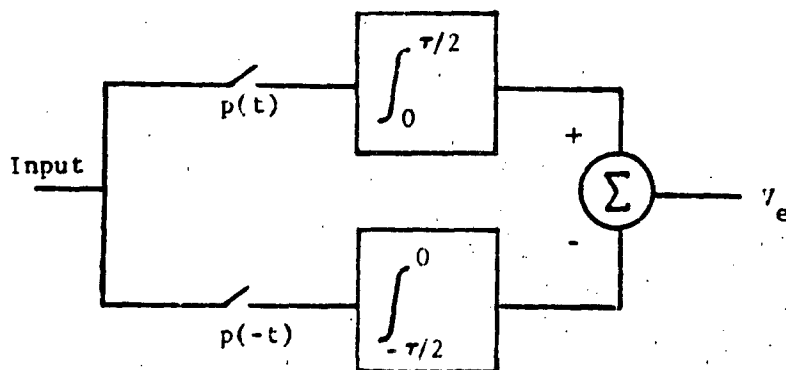


Fig 15. Range Gate Model $\left[p(t) = k, 0 < t < \tau/2; p(t) = 0, \text{ elsewhere} \right]$ (Golden, 1983:Fig. 7-34)

Range Servo. The repositioning of the sampling time (T_0) is performed electronically by a Type II servo system (Golden, 1983:322). The range servo has no mechanical constraints and has a transfer function of:

$$G(s) = K(s + w_2) / (s^2 w_2) \quad (19)$$

where $K = \frac{w_n^2}{n}$ and $w_2 = w_n/2\xi$.

The step response and rise time for this servo system are given by (ibid:322):

$$R_{r_o}(t) = 1 - \frac{1}{\sqrt{1-\xi^2}} \exp[-\xi w_n t] \cos\left[w_n \sqrt{1-\xi^2} t + \cos^{-1} \sqrt{1-\xi^2}\right] \quad (20)$$

$$t_r = \frac{\pi - 2\cos^{-1} \sqrt{1-\xi^2}}{w_n \sqrt{1-\xi^2}} \quad (21)$$

A linear model of this system is shown in Figure 16.

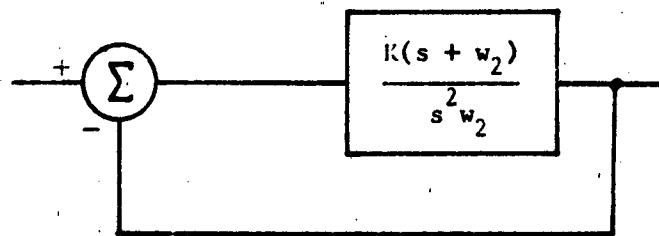


Fig 16. Type II Range Servo

Angle Tracking. Angle tracking in an SMC radar is accomplished in much the same way as in a conical scan radar. As stated previously, an error signal is generated in an SMC radar by subtracting the main and auxiliary channel signals. After range processing, this error signal is then used to drive antenna positioning servo-systems in both azimuth and elevation.

To generate the signals necessary to properly drive each servo, the error signal, filtered at the antenna scan frequency, is mixed with a reference signal from the antenna (See Figure 17). By low-pass filtering the outputs from the mixers, a dc error signal is produced to

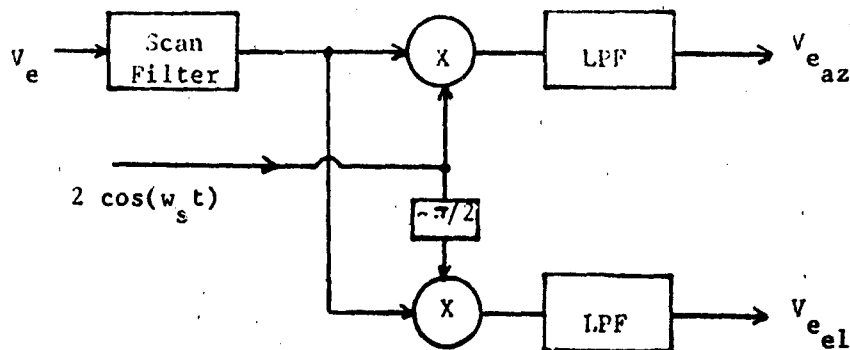


Fig 17. Angle Error Voltage Generation (Golden,1983:Fig. 7-8)

Angle Servo. Antenna repositioning is performed mechanically in both azimuth and elevation by improved Type I servos. Since both servos are similiar, only one analysis is needed.

An improved Type I servo-system has a transfer function of (ibid: 319):

$$G(s) = K(s+w_2) / [s(s+w_1)w_2] \quad (22)$$

where $K = w_n^2$ and $2\xi w_n = w_1 + K/w_2$. (The range servo has the same transfer function with $w_1 = 0$.)

The step response for this system is (ibid:320):

$$\theta_{A_o}(t) = 1 - \frac{\exp(-\xi w_n t)}{\sqrt{1-\xi^2}} - \sqrt{1-(w_1/w_2)} \cos[w_n \sqrt{1-\xi^2} t - \phi] \quad (23)$$

where:

$$\phi = \tan^{-1} \left[\frac{(w_1/w_n) - (w_n/w_2)}{2\sqrt{1-\xi^2}} \right] \quad (24)$$

The rise time is:

$$t_r = \frac{\pi - \tan^{-1} \left[\frac{(w_1/w_n) + (w_n/w_2)}{2\sqrt{1-\xi^2}} \right]}{w_n \sqrt{1-\xi^2}} + \phi \quad (25)$$

III. Centroid Tracking Model

Simple Tracking Model

In a simple tracking radar scenario, modeling the probability that chaff produces breaklock is as described in an article in the International Countermeasures Handbook (ICH, 1981:345-347). The aircraft is considered a point target and is being tracked by the radar and occupies the center of the radar resolution cell. After the chaff is dispensed, the radar tracks the power centroid of the combined return of the chaff and that of the aircraft, as long as both remain within the same radar resolution cell. As the aircraft and chaff separate due to a difference in speeds, the radar locks onto either the chaff or the aircraft, depending on which remains within the resolution cell.

In determining which target remains in the radar's resolution cell, the power centroid must be tracked and its position compared to the positions of the two targets. The power centroid lies on a line between the aircraft and the chaff cloud centroid. The position on that line is given by the "center of gravity" of the chaff and aircraft return powers.

If the aircraft is assumed to be in straight and level flight, the three-dimensional SWC radar resolution cell can be reduced to a rectangle at large ranges (See Figure 18). The power centroid's position, and therefore the position of the center of the resolution cell, along the aircraft's velocity vector, relative to the chaff location, is given by (Bueche, 1975:133):

$$x_{\text{cen}} = (x_{\text{AC}} - x_{\text{CHF}}) \frac{P_{\text{AC}}}{P_{\text{T}}} \quad (26)$$

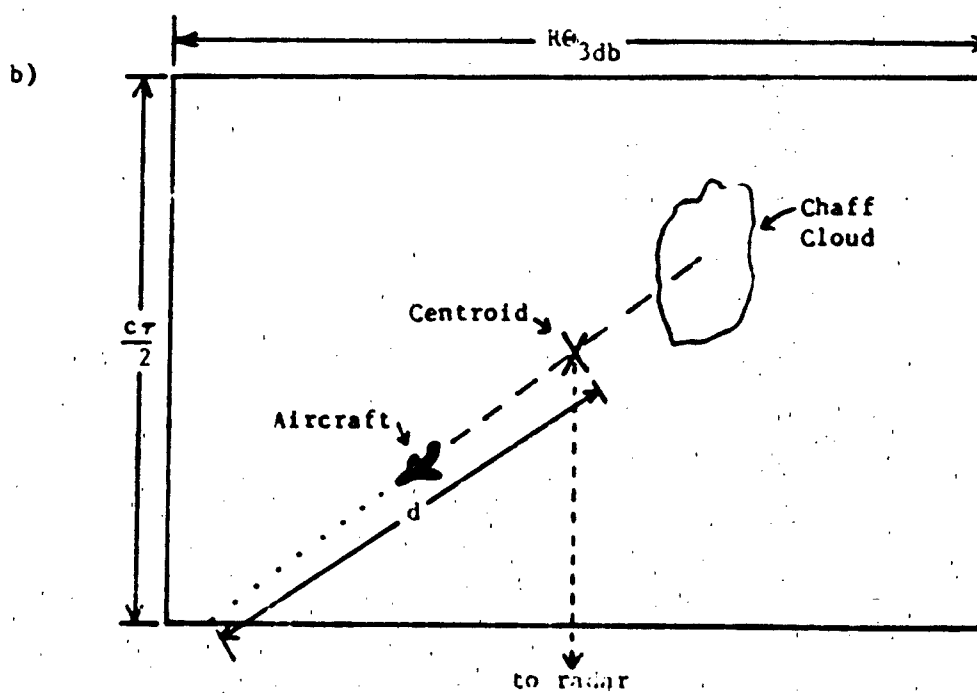
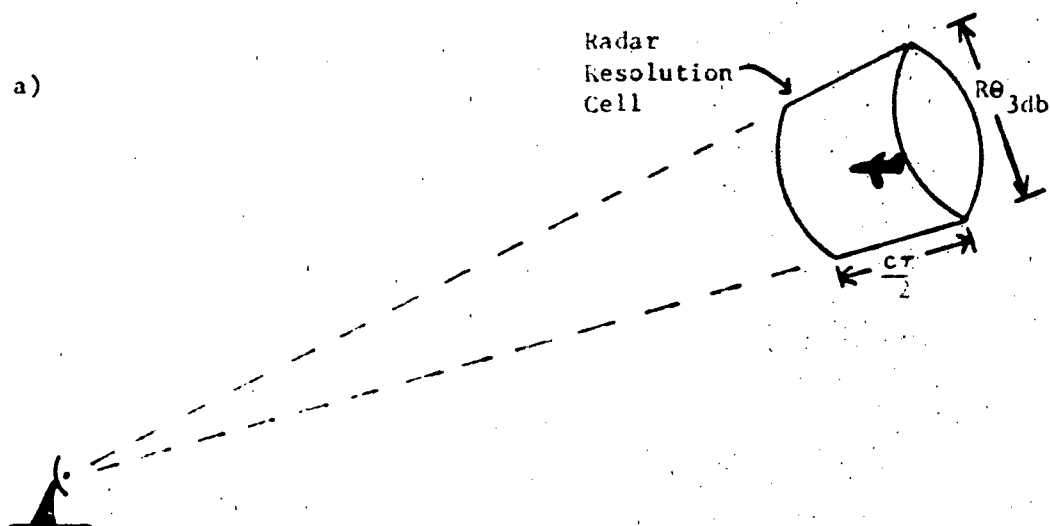


Fig 18. Radar Resolution Cell a) 2-dimensional ; b) 3-dimensional

where P_{AC} is the aircraft return power and P_T is the sum of the chaff and aircraft return powers.

In order to transfer radar-lock from the aircraft to the chaff, the aircraft must leave the radar resolution cell before the chaff. Referring to Fig. 18b, when the aircraft is at distance d from the centroid, the chaff must be closer to the power centroid than the aircraft. The probability of achieving breaklock is, therefore, not only a function of the chaff and aircraft return power, but also of aircraft velocity and radar resolution cell dimensions.

The power returned to the radar by the aircraft and the chaff is determined by the radar range equation (Skolnik, 1980:63):

$$P_r = \frac{P_t G \Lambda_e \sigma}{(4\pi)^2 R^4 L_s} \quad (27)$$

Assuming the distance between the aircraft and chaff to be very small in comparison with the range to the radar, equation (27) becomes, for chaff:

$$P_r = k \sigma_{CHF} / L_s \quad (28)$$

while for the aircraft:

$$P_r = k \sigma_{AC} / L_s \quad (29)$$

where k is a constant and L_s are system losses.

The only system loss that does not occur equally to both the chaff and aircraft return signals (assuming their difference in position is extremely small compared to the distance to the radar) is the beam-

shape loss. Beam-shape loss occurs due to the fact that the transmitted power is not a constant over the radar resolution cell, but varies due to the antenna power pattern. The antenna power pattern can be approximated by (ibid:58):

$$G = \exp(-2.78 \theta^2 / \theta_{3db}^2) \quad (30)$$

where θ is the angle from the beam center and θ_{3db} is the two-way 3db beamwidth. The position of the target within the resolution cell will, therefore, determine the loss due to beam-shape.

The beam-shape within an SWC radar resolution cell is shown in Figure 19, with the center of the cell at the half-power point and the edges representing a gain of unity. Using y as the distance to the closest edge of the cell and w as the width of the cell, equation (30) becomes:

$$G_{SWC} = \exp(-2.78 y^2 / w^2) \quad (31)$$

The power returned from a target is now given by:

$$P_r = k G_{SWC} \sigma \quad (32)$$

The power returned from the aircraft is now only a function of the distance from the side of the resolution cell, while the return power of the chaff cloud is dependent on that distance plus the time-varying RCS of equation (11):

$$\sigma(t) = \sigma_{max} [1 - \exp(-t/\tau_0)]$$

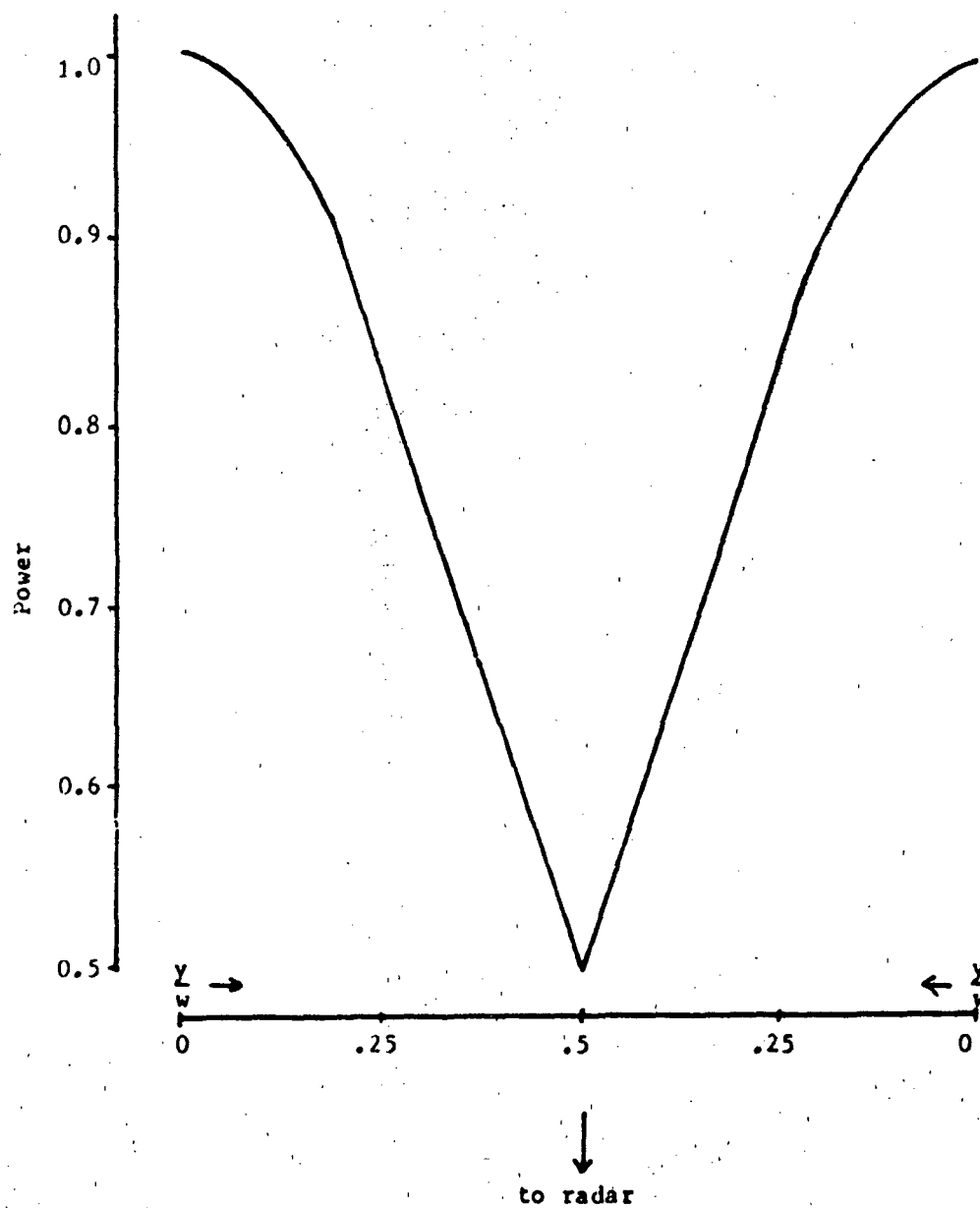


Fig. 19. SWC Power Pattern (within a resolution cell).

Aircraft velocity and radar resolution cell dimensions determine the position of the targets and constrain the time of the encounter, therefore, limiting the chaff RCS. By letting:

$$\sigma_0 = \sigma(t) = \sigma_{\max} [1 - \exp(-t/\tau_0)]$$

and substituting into equation (4), we observe that the distribution of the chaff RCS becomes an important factor in calculating the probability of breaklock.

Breaklock occurs when the chaff return power is larger than the aircraft return power, while both targets remain within the same radar resolution cell. The probability of achieving breaklock is therefore given as:

$$p(bl) = p(P_{r_{CHF}} > P_{r_{AC}}) \quad (33)$$

Substituting equations (4) and (32) into (33) yields:

$$p(bl) = \frac{G_{CHF}}{G_{AC}} \int_{\sigma_{AC}}^{\infty} \left[\frac{1}{\sigma_0} \right] \exp(-\sigma/\sigma_0) d\sigma \quad (34)$$

Integrating and substituting for σ_0 yields:

$$p(bl) = \frac{G_{CHF}}{G_{AC}} \exp \left[\frac{-\sigma_{AC}}{\sigma_{\max} [1 - \exp(-t/\tau_0)]} \right] \quad (35)$$

The probability of achieving breaklock is now a factor of time, where time is limited by the constraint that both targets remain within the same radar resolution cell.

MTI Radar Model

A block diagram of a typical Scan with Compensation tracking radar with MTI capability is shown in Figure 20. Previous analysis has shown that the SMC radar is basically a comparator which produces an error voltage to drive the servo tracking system. If it is assumed that the radar is tracking a point between two targets within a single resolution cell, the error voltage generated by the radar is simply a function of which channel (and therefore which target) contains the most return power. The probability of achieving breaklock, neglecting servo response time, therefore, is given by equation (33). The return powers, however, are now affected by the receiver structure.

The return power from each target, at the comparator is given by equation (32) modified by the gain of the MTI filter. (All other receiver front end gains are assumed equal for both channels and will therefore cancel at the comparator. With normal intermediate frequency automatic gain control response times being on the order of several pulse repetition intervals, the AGC gain will be slow in affecting the power level. AGC gain will be assumed equal for both channels and will, therefore, be neglected.) The power out of an MTI filter is given as (Cooper, 1967:112):

$$P_{O, TI} = \frac{1}{2\pi} \int_{-\infty}^{\infty} X(\omega) |H(\omega)|^2 d\omega \quad (36)$$

where $X(\omega)$ and $H(\omega)$ are, respectively, the power spectrum of the input signal and the transfer function of the MTI filter.

The power spectrum of the aircraft is a delta function, located at the doppler frequency, while the spectrum of the chaff has the

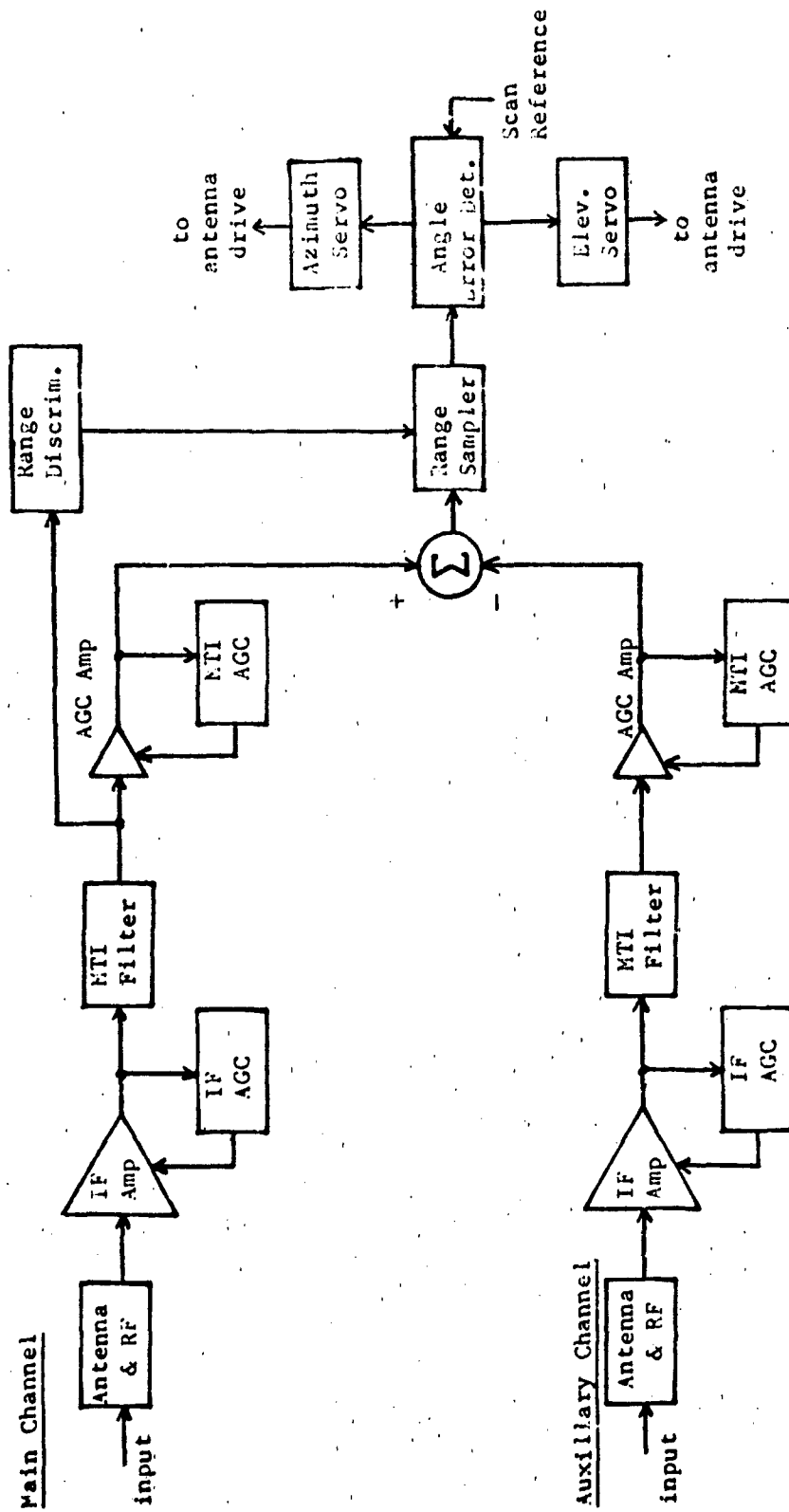


Fig 20. Scan with Compensation Radar

Gaussian properties discussed earlier. Since neither function is dependent on σ , the gain factor of the MTI filter can be moved outside the integral of equation (34), yielding the following expression for probability of breaklock:

$$p(bl) = \frac{G_{CHF} P_{NTI/CHF}}{G_{AC} P_{MTI/AC}} \exp \left[\frac{-\sigma_{AC}}{\sigma_{max} (1 - \exp(-t/\tau_{\sigma}))} \right] \quad (37)$$

where P_{NTI} is normalized to the MTI filter input power.

IV. Model Simulation

The model developed in the previous chapter will now be simulated on a computer. Quick examination of the model reveals that a time domain implementation is most appropriate. The simulation will require continuous calculation of the quantities of equation (37) while maintaining the constraint that both the aircraft and chaff remain within the same radar resolution cell.

Input Variables

The simulation must be flexible enough to accommodate aircraft, chaff, and scenario parameters as desired by the user. Radar parameters that can be varied by an operator and those that vary within a certain radar configuration must also be included. This will allow the user to determine correctly the probability of breaklock for a variety of situations.

Input variables needed to describe the aircraft are its radar cross section, velocity, and initial range to radar. As stated previously, the aircraft RCS will be assumed a constant, to be specified by the user prior to simulation. For example, one can specify the average RCS over all aspect angles. Since the model assumes that the aircraft must remain in straight and level flight, it will not be possible to vary the aircraft velocity while the simulation is in progress.

Input variables to describe chaff are maximum RCS, bloom rate, deceleration rate, and variance of the power spectrum. As stated in Chapter III, the value of σ_{\max} will be the average of the measured RCS

for the particular chaff type/design that is to be used. This assumption is based on a study of chaff cloud RCS measurements (Fuskar, 1975: 50-55), where data reveals that chaff cloud RCS values rarely meet their designed, or even consistent, RCS values. Bloom rate and deceleration rate are input variables whose values depend upon the type of cartridge and chaff used. Because of certain varying factors, specification of these values is best left to the discretion of the user. Although calculation of the variance of the chaff cloud spectrum can be accomplished as shown in Chapter II, in an effort to simplify the simulation and reduce run time, the variation will be entered as a user specified input.

Radar parameters assumed to be operator adjustable, or variable within a particular radar configuration, are required simulation inputs. These are pulse width, antenna beamwidth, operating frequency, and pulse repetition frequency. The pulse width and antenna beamwidth determine the dimensions of the radar resolution cell, and, consequently, the probability of attaining breaklock. The PRF, as will be shown later, will affect the response of the MTI filter. The radar parameters will be held constant during the simulation, although a human operator may alter them in practice. No accurate model of the human operator exists, at present, and no attempt to create one for this simulation will be attempted.

A complete list of simulation inputs is contained in Table 3.

Locations

The simulation of the aircraft/chaff/tracking radar encounter must constantly update the positions of the aircraft, chaff cloud cen-

Table 3. Simulation input parameters describing the aircraft, chaff, and radar.

Model	Input	Units
Aircraft	RCS	meters ²
	speed	Nmi/hr
	initial range	kilometers
	angle off boresight	radians
Chaff	maximum RCS	meters ²
	bloom rate	seconds
	deceleration rate	m/sec ²
	spectrum variance	Hz
Radar	pulse width	μ sec
	antenna beamwidth	radians
	operating frequency	GHz
	PRF	KHz

troid, and combined power centroid within the radar resolution cell.

The antenna gain and the time limit of the encounter are functions of these positions.

The time interval at which position updates occur must be large enough to allow for fast simulation run times and small enough to restrict target movements to reasonable levels. Sampling at the scan interval (~ 0.04 seconds) would allow an aircraft traveling at 600 knots to move 12 meters between calculations. While this distance may be less than the aircraft's actual length, it is larger than one-half the radar resolution cell depth for a 0.1μ sec pulse width. Therefore, if the aircraft had a radial velocity of 600 knots with respect to the radar, the target would be out of the resolution cell before the first

measurement was made.

At the other extreme, sampling at the pulse repetition interval could prove time consuming. With a 2KHz PRF (PRI = 0.0005 sec), a chaff cloud with a 0.5 second bloom rate would only reach 0.1 percent of its RCS. While these examples represent extreme cases, they are realizable. The simulation will be designed to sample at 0.005 second intervals, a compromise between the above extremes. Later analysis may require this interval to be modified, but in the interest of reducing the number of input variables, it will remain a fixed quantity.

By assuming the aircraft is in straight and level flight, and is not allowed to maneuver or accelerate during the simulation, the scenario is simplified to two dimensions, as stated in Chapter III. Disregarding the sign of the doppler shift, the aircraft's angle of attack (off boresight) can be restricted to $0^\circ \leq \theta_A \leq 90^\circ$. This contains the aircraft's movement to one quadrant of the resolution cell, being possible due to the symmetrical geometry of the "square" radar resolution cell.

The scenario has now become a function of the aircraft's radial and tangential velocity components (with respect to the radar). The aircraft's velocity vector is now reduced to its respective components, as shown in Figure 21, where:

$$|v_{\text{radial}}| = |v| \cos \theta_A \quad (38)$$

$$|v_{\text{tang}}| = |v| \sin \theta_A \quad (39)$$

Similarly, using equation (11), chaff velocity is:

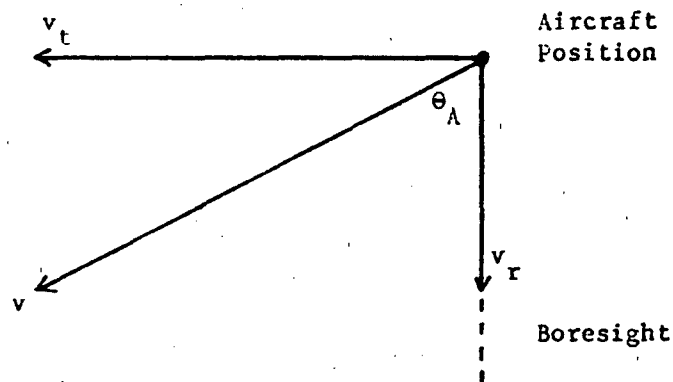


Fig 21. Aircraft Radial and Tangential Velocity Components

$$|v_{\text{rad}}| = |v| \exp[-t/\tau_v] \cos \theta_A \quad (40)$$

$$|v_{\text{tan}}| = |v| \exp[-t/\tau_v] \sin \theta_A \quad (41)$$

Since τ_v is expressed in seconds and the chaff deceleration input in meters/second², the input variable must be converted to the proper units. At time $t = 4\tau_v$, $\exp[-t/\tau_v]$ reaches a value of 0.0183. Therefore asserting that zero velocity is reached at $t = 4\tau_v$ will create an error of less than 2 percent. Assuming the 2 percent error to have only a negligible affect on the calculations, the conversion of units can continue.

For constant acceleration, the velocity equation is (Bueche, 1975: 38):

$$v = v_0 + at \quad (42)$$

Setting $v = 0$ and solving for t yields:

$$t = v_o/a \quad (43)$$

where the sign is dropped assuming deceleration. Substituting $t = 4\tau_v$ into equation (43) yields a new deceleration constant of:

$$\tau_v = v_o/4a \quad (44)$$

Having the correct units, we now proceed.

The positions of the aircraft and chaff, with respect to the power centroid, can also be expressed in radial and tangential directions from the radar. The aircraft position, at time t , is given by:

$$x_{tAC} = (v_{tAC} - v_{tCHF})t \frac{P_{CHF}}{P_T} \quad (45)$$

$$x_{rAC} = (v_{rAC} - v_{rCHF})t \frac{P_{CHF}}{P_T} \quad (46)$$

The chaff location is given by:

$$x_{tCHF} = -(v_{tAC} - v_{tCHF})t \frac{P_{AC}}{P_T} \quad (47)$$

$$x_{rCHF} = -(v_{rAC} - v_{rCHF})t \frac{P_{AC}}{P_T} \quad (48)$$

The antenna gain can now be found, using the tangential distance to the centroid:

$$G_{AC} = \exp \left[-2.78 \frac{\left[\frac{w}{2} - |x_{tAC}| \right]^2}{w^2} \right] \quad (49)$$

$$G_{CHF} = \exp \left[-2.78 \frac{\left[\frac{w}{2} - |x_{t_{CHF}}| \right]^2}{w^2} \right] \quad (50)$$

where:

$$w = R\theta_{3db} \quad (51)$$

Since the simulation time is restricted due to the fact that both the aircraft and chaff must remain within the same radar resolution cell, target positions must also be compared to resolution cell dimensions. The simulation will terminate when the distance between the aircraft, or chaff, and the power centroid exceeds one-half the resolution cell size. Therefore, at each time interval, $|x_t|$ for both the aircraft and chaff will be compared to $R\theta_{3db}/2$, and $|x_r|$ for each will be compared to $c\tau/4$. If any value exceeds the limits, the simulation will be terminated and outputs created. The output probability of attaining breaklock will be that of equation (37), at a time t_1 , determined from the distance-to-cell dimension comparators.

MTI Response

With the exception of the relatively easy calculation of chaff RCS, the remaining calculation required of the simulation is that of the power out of the MTI filter. The output power is given by equation (36) as:

$$P_{o_{MTI}} = \frac{1}{2\pi} \int_{-\infty}^{\infty} X(w) |H(w)|^2 dw$$

where, for purposes of this simulation, $X(w)$ and $H(w)$ are the normal-

ized power spectrum of the target and the MTI filter response, respectively. Therefore, all that remains is to calculate the respective power spectra.

The power spectrum of the MTI filter is a function of the MTI filter design and, therefore, an internal radar characteristic. In order to simplify the simulation, yet make it applicable to a wide range of radar designs, a worst case (for chaff) design was created, using the double delay line canceler discussed in Chapter II.

The normalized amplitude response of the MTI filter incorporated into this simulation will be that of Figure 24. An MTI filter with this response displays the unity response characteristic of a staggered PRF system, but includes the slow initial rise of a single PRF double delay line canceler. A staggered PRF radar has a faster initial rise in the amplitude response due to the combination of initial responses from the

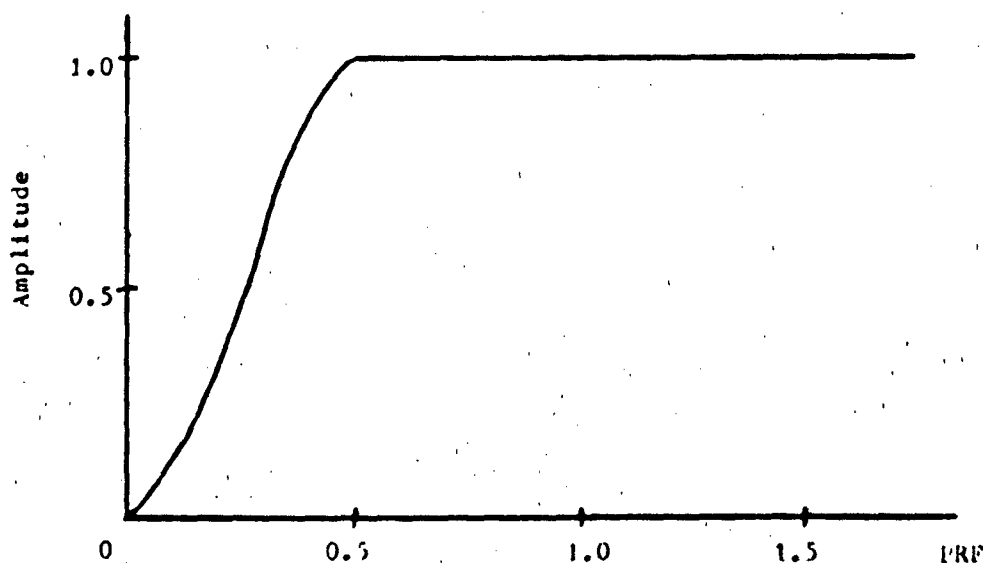


Fig. 22. Simulation MTI Filter Response (Amplitude)

different PRF's. The initial rise of Figure 22 is that of the lowest PRF used by the radar, therefore being somewhat slower than an actual staggered PRF response. This MTI filter response presents an obstacle to chaff in that targets with small doppler frequencies are attenuated, yet targets with large doppler frequencies are passed by the filter, with no effect due to doppler blind speeds.

The power spectrum of the MTI filter is now given by:

$$P(f) = \begin{cases} \sin^4(\pi f / \text{PRF}) & , f \leq \text{PRF}/2 \\ 1 & , f > \text{PRF}/2 \end{cases} \quad (52)$$

As stated in Chapter III, the power spectrum of the return signal from the aircraft will be a delta function, of height 1, at the doppler frequency of the aircraft. Substituting the results of equation (52) and the doppler frequency of the aircraft, as determined from equation (14), into equation (36) and solving, yields a normalized MTI filter gain for the aircraft return of:

$$P_{\text{O MTI/AC}} = \begin{cases} \sin^4 \left[\frac{2\pi f_o v_r}{c \text{PRF}} \right] & , v_r \leq \frac{c \text{PRF}}{4f_o} \\ 1 & , v_r > \frac{c \text{PRF}}{4f_o} \end{cases} \quad (53)$$

Since the aircraft is not allowed to alter its velocity vector during the simulation, the MTI gain factor will remain constant throughout the simulation.

The power spectrum of the chaff return signal was given in equation (13) as:

$$G(f) = G_o \exp \left[-\frac{(f - f_d(t))^2}{2\sigma_f^2} \right]$$

where the mean of the doppler return is:

$$f_d(t) = \frac{2f_0}{c} v_r \exp(-t/\tau_v) \quad (54)$$

and the value of the normalizing constant, G_0 , is determined to be (Papoulis, 1965:66):

$$G_0 = 1/\sqrt{2\pi\sigma_f^2} \quad (55)$$

the power spectrum of the chaff return is a function of time and the normalized MTI filter output must be recalculated for each time interval during the simulation, until the mean of the chaff cloud centroid doppler frequency reaches zero. When the mean of the doppler frequency equals zero, the chaff spectrum will reach a steady-state value, where it will remain for the duration of the simulation. From previous analysis of the deceleration constant, and the mean cloud doppler frequency, the chaff spectrum will attain a steady-state response at:

$$t = v_r/a \quad (56)$$

The normalized gain out of the MTI filter, due to the chaff return signal, can now be stated as a sum of integral equations. Equation (36) now becomes:

$$F_{0MTI/CHF} = 1/\sqrt{2\pi\sigma_f^2} \int_{-PRF/2}^{PRF/2} \sin^4(\pi f/PRF) \exp\left[-(f-f_d(t))^2/2\sigma_f^2\right] df +$$

$$\begin{aligned}
& 1/\sqrt{2\pi\sigma_f^2} \int_{PRF/2}^{\infty} \exp\left[-(f-f_d(t))^2/2\sigma_f^2\right] df + \\
& 1/\sqrt{2\pi\sigma_f^2} \int_{-\infty}^{-PRF/2} \exp\left[-(f-f_d(t))^2/2\sigma_f^2\right] df \quad (57)
\end{aligned}$$

Inserting the large chaff frequency variances, shown in Chapter II, into equation (13) result in a relatively small, broadband frequency spectrum. An attempt was made to equate this spectrum to the flat spectrum of white Gaussian noise, therefore rendering equation (57) a constant. The properties of the Gaussian curve prohibit this, however. From these properties, it can be shown (Soong, 1981:195) that approximately 98 percent of the energy of a Gaussian spectrum lies within 2.6 standard deviations of the mean. Using the smaller variance limit from the example in Chapter II, 98 percent of the energy would be concentrated within a bandwidth of less than 150 Hz. This small concentration of signal energy prohibits equating the chaff and Gaussian white noise spectra.

Equation (57) can be simplified, however, and its form can be reduced for certain cases. The last two lines of the equation are related to the error function and are equal for the case when $f_d(t) = 0$. For cases when the PRF > 500 Hz and $f_d(t) = 0$, these lines go to zero and by symmetry, equation (57) reduces to:

$$P_{o_{MTI/CHF}} = 2/\sqrt{2\pi\sigma_f^2} \int_0^{PRF/2} \sin^4(\pi f/PRF) \exp\left[-f^2/2\sigma_f^2\right] df \quad (58)$$

Equation (58) can be implemented during the simulation as $f_d(t)$ goes to zero to reduce run time.

Utilizing the calculations outlined in this chapter, a simulation can now be constructed. Since the radar model has been reduced to an antenna gain pattern and an MTI filter, the simulation, flowcharted in Figure 23, will not produce an exact probability of breaklock. It can be used, however, to indicate how changing certain parameters can identify the effect of that change on the probability of attaining breaklock. By simply varying one input parameter over a specified range and plotting the simulation output versus that input parameter, one obtains a graph of how that parameter affects the probability of attaining breaklock.

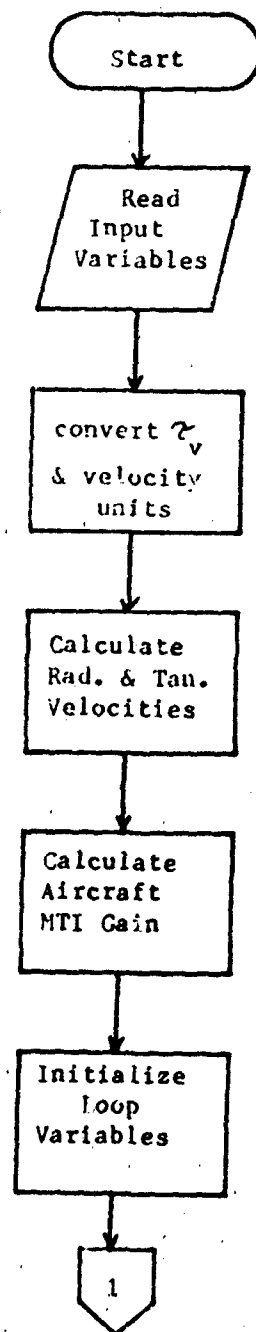


Fig 23. Simulation Flow Chart (page 1 of 3)

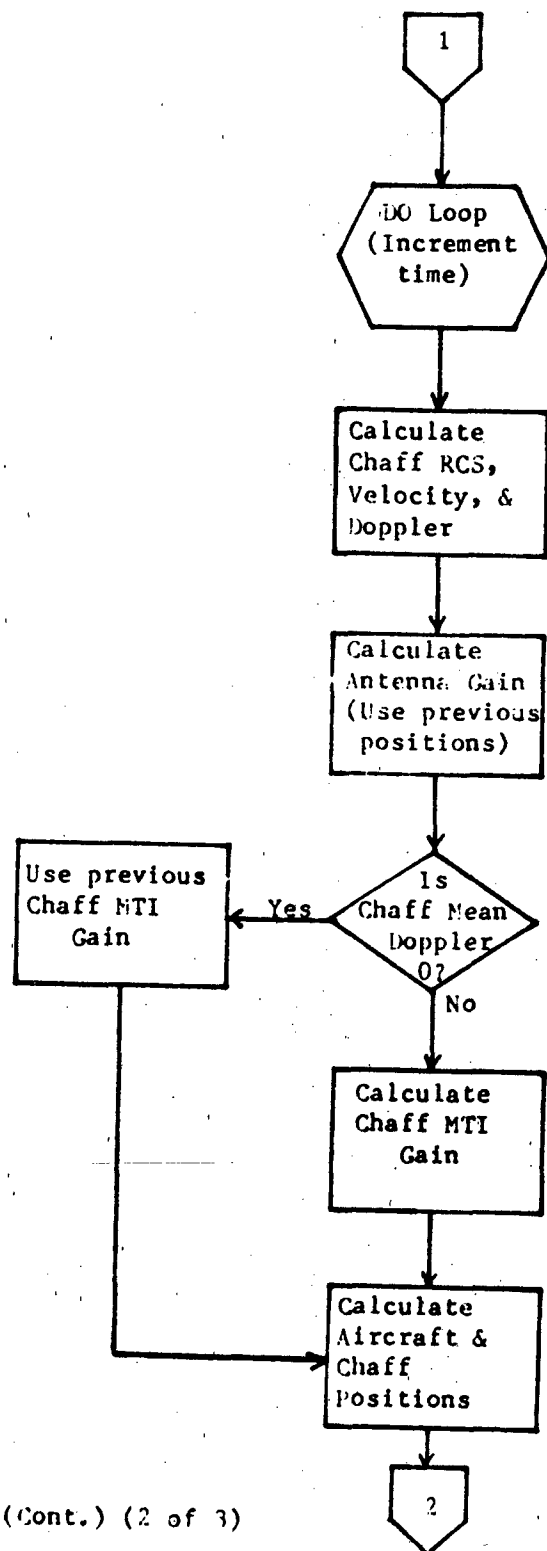


Fig. 23. (Cont.) (2 of 3)

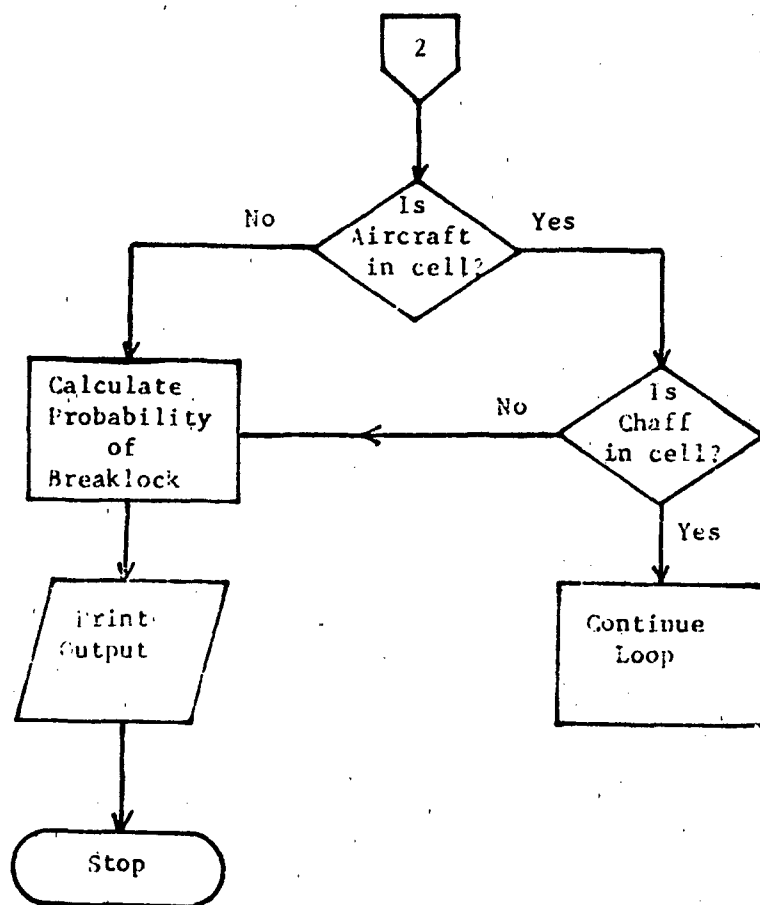


Fig 23. (Cont.) (3 of 3)

V. Conclusions and Recommendations

Maximizing the effectiveness of chaff use, in a self-protective role, is one method to increase the survivability of combat aircraft. Allowing an aircraft commander to increase chaff effectiveness through apriori knowledge of the best tactics to employ in an aircraft-chaff-tracking radar encounter will increase the chance of mission success. This thesis has produced a simulation that allows the user to attain this apriori knowledge by determining how certain parameters affect the probability of attaining breaklock.

"The most dominant factor in chaff effectiveness is the radar cross section of the chaff compared to the airplane at the time when the airplane and chaff are in the same resolution cell and the chaff has sufficient velocity to defeat the MTI and pulse-doppler filters." (Bang, 1979:148). The simulation created in Chapter IV utilizes these factors and constraints to chart chaff effectiveness. While the author concedes the fact that many factors affect chaff performance, in an effort to reduce simulation run time and complexity, those "other" factors have been neglected due to their small individual affect on the outcome.

Results from two simulation runs are plotted in Figures 24 and 25. The inputs for these runs are contained in Table 4.

Figure 24 shows the effect of varying the chaff RCS on the probability of breaklock. The relatively small values of $p(b1)$ occur because the MTI filter passes the entire aircraft return signal and highly attenuates the chaff return due to the situation geometry. Note that the curve tends toward $(1 - \exp(-x))$. This implies that there is a point,

Table 4. Simulation inputs.

	Input	Simulation #1	Simulation #2
Aircraft	RCS (m^2)	10	10
	speed (knots)	500	500
	range (km)	10	10
	angle (rad.)	0	varied
Chaff	RCS (m^2)	varied	50
	bloom rate (s)	0.1	0.1
	decel. rate (m/s^2)	1000	1000
	variance (Hz)	3700	3700
Radar	pulse width (μs)	5	5
	beamwidth (rad.)	0.26	0.26
	RF (GHz)	7.0	7.0
	PRF (KHz)	2.0	2.0

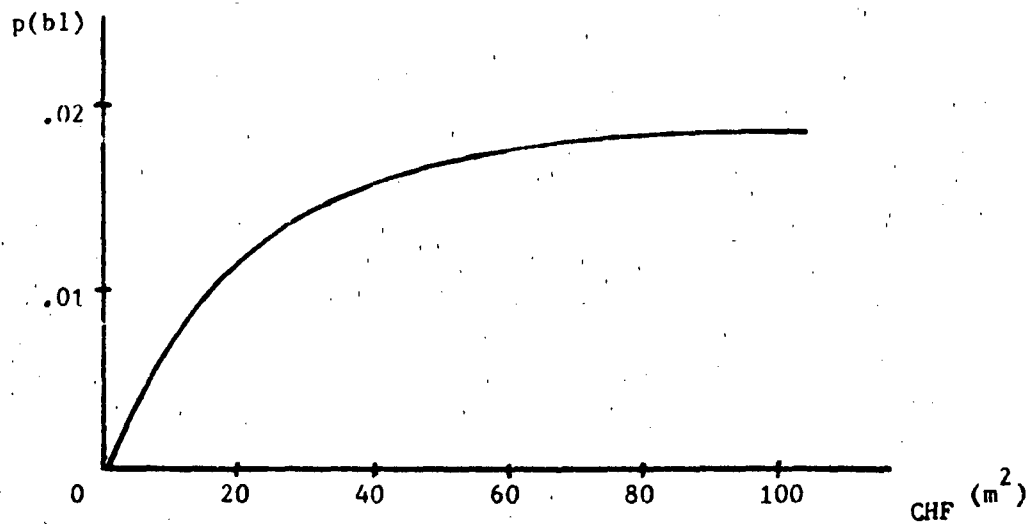


Fig 24. Simulation #1 Results. Chaff RCS vs. Probability of Breaklock

whereafter increasing the chaff RCS produces almost no increase in the probability of breaklock. As one would expect, the smoothness of the curve also indicates that MTI response and antenna gain are not affected by the chaff RCS in this situation.

Figure 25 plots the effect of varying the direction of the aircraft's velocity vector on the probability of breaklock. Until $\theta = 85^\circ$, the variation in $p(b1)$ is due mainly to the difference in antenna gain for the two targets. After 85° , the MTI filter begins to attenuate the aircraft's return due to its small doppler frequency, until, at $\theta = 90^\circ$, $p(b1) = 1$. From Figure 25 it can be implied that a maneuver through a plane perpendicular to the boresight will produce breaklock; that is if the maneuver can be accomplished while the chaff and aircraft remain within the same resolution cell.

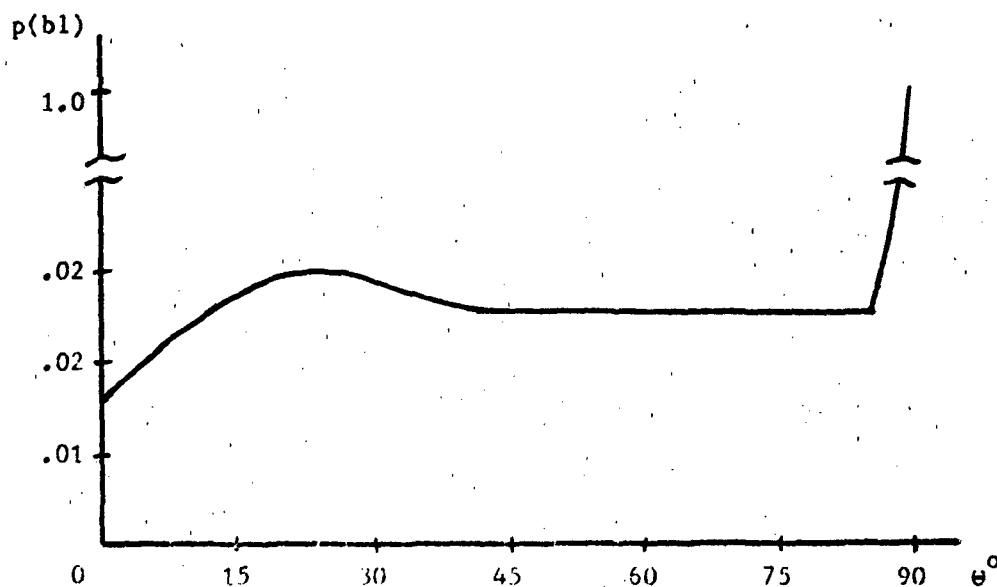


Fig 25. Simulation #2 Results. Angle off Boresight vs. Probability of Breaklock.

Recommendations

MTI- It is obvious from the results obtained from simulation runs that the "ideal" MTI filter response incorporated in the simulation must be modeled more realistically. One solution is to include several different filter responses in the radar model. This would allow the user the choice of the filter that best represents the response desired in the simulation.

AGC- Further research could determine the actual effect of AGC on chaff effectiveness. Amplification of the relatively small chaff return signal, immediately upon dispersion, could combine with the non-zero mean doppler frequency spectrum to enhance chaff's effectiveness. However, an effort must be made to reduce the additional complexity and run time caused by a radar system employing several different types of AGC.

Servo Systems- Ideal servo systems over-react to chaff, therefore, allowing chaff to more readily break lock than would a less responsive system (ICH, 1981:347). Modification to include a more "realistic" servo response time would greatly improve the accuracy of the simulation.

Maneuvering- Further modification of the simulation to include 3-dimensional maneuvers is necessary to properly model the aircraft-chaff-radar encounter. A vertical dive puts the aircraft at near-zero radial velocity, greatly reducing its return doppler shift, therefore reducing the aircraft's signal power at the output of the MTI filter.

SCARE- The requirement for a precise figure for probability of breaklock requires the use of a simulation with the complex modeling employed in SCARE. An effort should be attempted to modify SCARE to

produce this desired output.

Bibliography

- Bang, Lt Steven B. The Effectiveness of Self-Protective Chaff Against Radar, VTI, Resolution and Control Servos. MS Thesis, AFIT/GE/EE 79-6. School of Engineering, Air Force Institute of Technology (AU), Wright-Patterson AFB, OH. December 1979. (AD-B043 824L)
- Barlow, Edward J. "Doppler Radar", Proceedings of the I.R.E., 37: 340-355 (Apr 1949).
- Barrick, Donald E. and others. Radar Cross Section Handbook, Volume 2. New York: Plenum Press, 1970.
- Bueche, Fredrick J. Introduction to Physics for Scientists and Engineers (Second Edition). New York: McGraw-Hill Book Company, 1975.
- Cooper, George R. and Clare D. McGillem. Methods of Signal and System Analysis. New York: Holt, Rinehart, and Winston Inc., 1967.
- Golden, Maj August, Jr. Radar Electronic Warfare. Wright-Patterson AFB: AFIT Press, 1983.
- ICH, "Aircraft Chaff: Centroid Effects", International Countermeasures Handbook, 7th Edition: 345-347 (1982).
- Johnson, Capt Thomas W. Lecture materials distributed in EE 5.73, Electronic Warfare. School of Engineering, Air Force Institute of Technology (AU), Wright-Patterson AFB, OH, December 1983.
- Nathanson, Fred E. Radar Design Principles. New York: McGraw-Hill Book Company, 1969.
- Papoulis, Athanasios. Probability, Random Variables, and Stochastic Processes. New York: McGraw-Hill Book Company, 1965.
- Fuskar, Robert J. Chaff Cloud RCS Studies and Measurements Using a High Resolution Radar. 1 June 1973-1 September 1974. Work Unit 7633-1332. Avionics Laboratory, AFAL/FAF, Air Force Wright Aeronautical Laboratory, Wright-Patterson AFB OH, July 1975. (AD-B007252L)
- Pyati, Vittal P. "On the Convergence of the Scattering Statistics of Finite Number of Randomly Oriented Dipoles to Rayleigh", Proceedings of IEEE, 63: 985-986 (Jun 1975).
- Skolnik, Merrill I. Introduction to Radar Systems (Second Edition). New York: McGraw-Hill Book Company, 1980.
- Soong, T.T. Probabilistic Modeling and Analysis in Science and Engineering. New York: Wiley and Sons Inc., 1981.

Stutzman, Warren L. and Gary A. Thiele. Antenna Theory and Design. New York: Wiley and Sons Inc., 1981.

Vakin, S. and L. Shustov. Principles of Jamming and Electronic Reconnaissance, Volume 11, FTD translation. Foreign Technology Division, Wright-Patterson AFB OH, 1969. (AD 692643)

Van Brunt, Leroy B. Applied ECM, Volume 2. Dunn Loring VA: EW Engineering Inc., 1982.

VITA

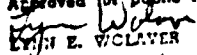
Lieutenant Robert J. Kohrs was born on 27 October 1954 in Toledo, Ohio. He graduated from high school there, in 1972, and entered the USAF as a Ground Radio Communications Equipment Repairman. Upon discharge in May 1976 he attended the University of Toledo. He received the degree of Bachelor of Science in Electrical Engineering in June 1982. Upon completion of OTS, he received a commission in the USAF in September 1982. He was assigned as a program manager for the College Senior Engineering Program until he entered the School of Engineering, Air Force Institute of Technology, in June 1983.

Permanent Address: 4214 Fairview Drive
Toledo, Ohio 43612

UNCLASSIFIED

SECURITY CLASSIFICATION OF THIS PAGE

REPORT DOCUMENTATION PAGE

1. REPORT SECURITY CLASSIFICATION UNCLASSIFIED			1b. RESTRICTIVE MARKINGS	
2a. SECURITY CLASSIFICATION AUTHORITY			3. DISTRIBUTION/AVAILABILITY OF REPORT Approved for public release; distribution unlimited.	
2b. DECLASSIFICATION/DOWNGRADING SCHEDULE			5. MONITORING ORGANIZATION REPORT NUMBER(S)	
4. PERFORMING ORGANIZATION REPORT NUMBER(S) AFIT/GE/ENG/84D-54			7a. NAME OF MONITORING ORGANIZATION	
6a. NAME OF PERFORMING ORGANIZATION School of Engineering		6b. OFFICE SYMBOL (If applicable) AFIT/ENG	7b. ADDRESS (City, State and ZIP Code)	
6c. ADDRESS (City, State and ZIP Code) Air Force Institute of Technology Wright-Patterson AFB, Ohio 45433			9. PROCUREMENT INSTRUMENT IDENTIFICATION NUMBER	
8a. NAME OF FUNDING/SPONSORING ORGANIZATION		8b. OFFICE SYMBOL (If applicable)	10. SOURCE OF FUNDING NOS.	
8c. ADDRESS (City, State and ZIP Code)			PROGRAM ELEMENT NO.	PROJECT NO.
11. TITLE (Include Security Classification) See Box 19			TASK NO.	WORK UNIT NO.
12. PERSONAL AUTHOR(S) Robert J. Rohrs, B.S., 1Lt, USAF				
13a. TYPE OF REPORT MS Thesis		13b. TIME COVERED FROM _____ TO _____	14. DATE OF REPORT (Yr., Mo., Day) 1984, December	
15. PAGE COUNT 71				
16. SUPPLEMENTARY NOTATION				
17. COSATI CODES			18. SUBJECT TERMS (Continue on reverse if necessary and identify by block number)	
FIELD 17	GROUP 04	SUB. GR.	Electronic Countermeasures, Chaff, Radar Tracking	
19. ABSTRACT (Continue on reverse if necessary and identify by block number) Title: AN EMPIRICAL SELF-PROTECTION CHAFF MODEL Thesis Chairman: Dr. Vittal P. Pyati				
<div style="text-align: right;"> <p>Approved for public release IAW AFR 190-17.  LYNN E. WCLAVER 25 Feb 85 Dean for Research and Professional Development Air Force Institute of Technology (AFIT) Wright-Patterson AFB OH 45433</p> </div>				
20. DISTRIBUTION/AVAILABILITY OF ABSTRACT UNCLASSIFIED/UNLIMITED <input checked="" type="checkbox"/> SAME AS RPT. <input type="checkbox"/> DTIC USERS <input type="checkbox"/>			21. ABSTRACT SECURITY CLASSIFICATION UNCLASSIFIED	
22a. NAME OF RESPONSIBLE INDIVIDUAL Dr. Vittal P. Pyati, Asst. Professor			22b. TELEPHONE NUMBER (Include Area Code) (513)255-2024	22c. OFFICE SYMBOL AFIT/ENG

DD FORM 1473, 83 APR

EDITION OF 1 JAN 73 IS OBSOLETE.

UNCLASSIFIED
SECURITY CLASSIFICATION OF THIS PAGE

UNCLASSIFIED

SECURITY CLASSIFICATION OF THIS PAGE

This thesis produced a simulation capable of charting the effectiveness of chaff used in the self-protective mode. Simulation results can be used to determine which type/design of chaff/chaff canister will produce a greater probability of breaklock for a given scenario.

The radar included in this simulation is a Scan with Compensation tracking radar. Variable parameters include pulse width, beamwidth, pulse repetition frequency, and operating frequency. An "ideal" MTI filter is incorporated into the model to negate the effects of MTI blind speeds.

Results of several simulation runs illustrate the effects of varying chaff radar cross section and aircraft velocity on the probability of attaining breaklock. Although aircraft maneuvers are not included in the simulation, conclusions as to how the probability of breaklock is affected can be made by varying the velocity vector.

UNCLASSIFIED

SECURITY CLASSIFICATION OF THIS PAGE

END

FILMED

5-85

DTIC